Aim and Scope

The objective of the *Journal of Residuals Science & Technology* (JRS&T) is to provide a forum for technical research on the management and disposal of residuals from pollution control activities. The Journal publishes papers that examine the characteristics, effects, and management principles of various residuals from such sources as wastewater treatment, water treatment, air pollution control, hazardous waste treatment, solid waste, industrial waste treatment, and other pollution control activities. Papers on health and the environmental effects of residuals production, management, and disposal are also welcome.

Editor-in-Chief

P. Brent Duncan
Department of Biology
University of North Texas
Denton, TX, USA
pduncan@unt.edu

Editorial Advisory Board

C O N T E N T S

Research

Recycling Oily Sludge Pyrolysis Residues as Nano-adsorbents

BING HOU[1,*], SHUIXIANG XIE[2], MIAN CHEN[1], CHUAN LIANG[1], HAO DENG[2], RONGSHA WANG[2]
and GUANGQUAN LIU[2]

[1]College of Petroleum Engineering, China University of Petroleum (Beijing), China, 102249
[2]CNPC Research institute of Safety & Environment Technology, Beijing, China, 102206

ABSTRACT: Oily sludge is a major oily waste originating from the oil refining industry production process. It is very difficult to handle and may harm portions (i.e., ecosystems and human health) of the environment. Oil and gas may be separated from oily sludge and economically recovered by pyrolysis technology. However, the by-product residue of pyrolysis would likely contribute to secondary pollution if a disposal method was not competent. A novel nano-adsorbent, NMA-12, was developed by synthesization between a supermolecule compound and an oily sludge pyrolysis residue with participation from chemically modified nanometer materials. Static adsorption and desorption kinetic characteristics of the adsorbent (NMA-12) were studied with Congo Red as the test adsorbate. Results suggest adsorption equilibrium time was approximately 150 minutes and that the apparent adsorption rate constant of Congo Red was k_{298} = 0.02 s^{-1}. Desorption volume of Congo Red at the same time was greater in stripping liquid where it reached 80.7% versus in pure water. This research was devoted to finding a feasible technology for treatment of oily sludge pyrolysis residues as a means of resource recycling.

INTRODUCTION

THE refining industry generates more than 100×10^7 Kg of oily sludge in China per year posing a daunting environmental challenge. Also, there is most likely more waste generated than this. Depending on source and composition characteristics, oily sludge can be classified according to four major categories [1,5,6]. The first type of oily sludge comes from cleaning tanks from the production stream for the oil gathering and processing system. It is mainly composed of sand, clay, water, and a high ratio of oil. Sand concentration is decided by lithology within reservoirs. The second type of oily sludge comes from cleaning storage tanks and is mainly composed of fine clay, water, and a high ratio of oil with serious emulsification. The third type of sludge is an oily residue from water treatment disposal systems and is mainly composed of fine clay, oil, water, macromolecular flocculating agents, and microbial slime. This sludge's characteristics are low oil content and severe emulsification. The last type of oily sludge is soil contaminated with oil and mainly consists of sand, oil, and water.

Today, reduction, recycling, and neutralization are guiding oily sludge treatment around the world [2,3,4,7,8,9,10,11]. Oily sludge is commonly treated by such methods as solvent extraction, incineration, biological processes, carbonization, and comprehensive utilization of oily sludge based on factors such as oily sludge profile. These technologies play a key role in the treatment process but they do have limitations.

Oily sludge pyrolysis residues are wastes mainly composed of coke, ash, and other inorganic matter and require further treatment. Secondary pollution is inevitable if these residues are treated inappropriately. This paper explores the possibility of utilizing oily sludge pyrolysis residues as a nanometer-scale adsorbent by exploiting characteristics of residues. This process may provide an example of innovative resource utilization.

OILY SLUDGE PYROLYSIS TECHNOLOGY

Developed from an understanding of sludge source and composition characteristics emerging from refinery waste water, the proposed pyrolysis flowchart for the treatment process is displayed in Figure 1. After dehydration, three sludges were separated into oil, water, wastes, and non-condensable gas by pyrolysis treatment whereby each component of the mixture un-
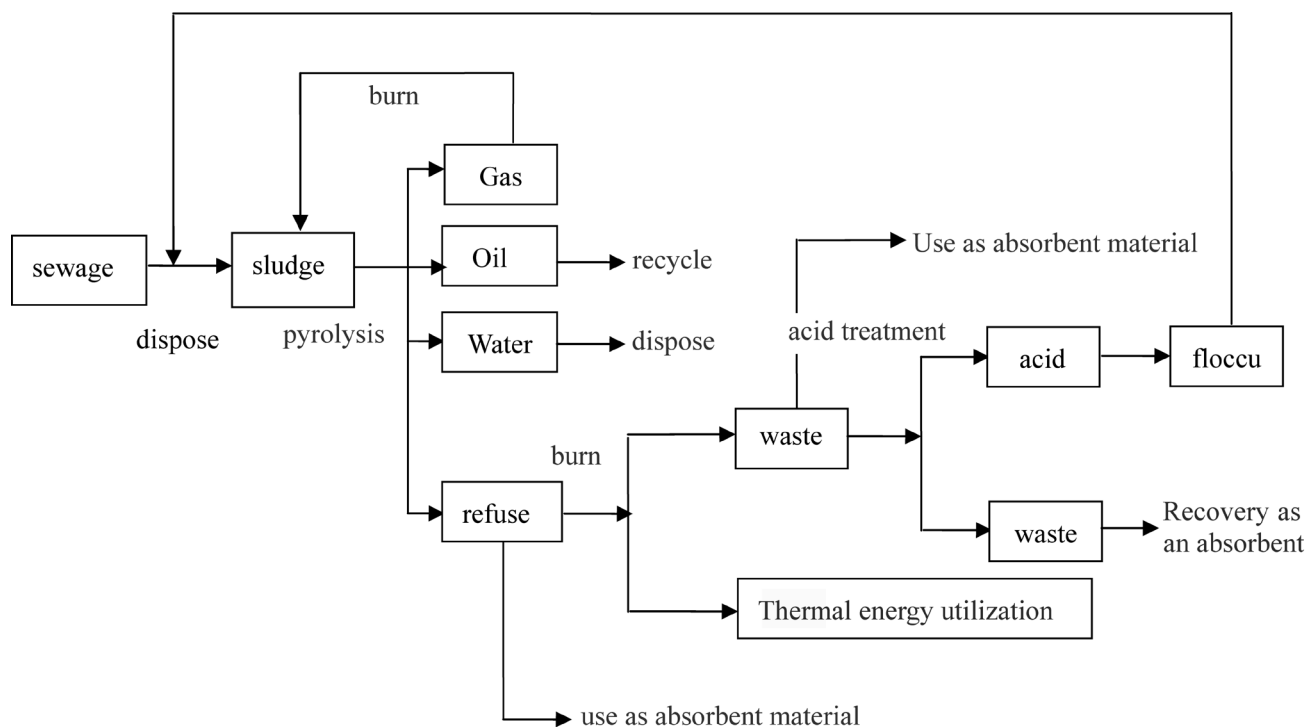
Figure 1. Oily sludge pyrolysis process flowchart.

derwent a different process. Pyrolysis oil was directly recycled. Water was disposed of via a wastewater treatment system once more. Non-condensable gas was used for pyrolysis fuel without further treatment. Wastes were used as an adsorbent and became a novel nano-scale adsorbent after further treatment.

EXPERIMENTS

Experimental Materials and Equipment

Reagents for this experiment were tetraethylorthosilicate (TEOS, industrial grade), Ammonium persulfate (APS, industrial grade), ammonia and water solution (25%) (chemically pure), N,N-Dimethylformamide, Dehydrated (N-DMF, analytical grade), anhydrous alcohol (analytical grade), acetonitrile (analytical grade), P-toluenesulfonyl chloride (PTSC, chemically pure), and Human integrin β2 ELISA Kit (β-CD, chemically pure) which was recrystallized twice with distilled water and vacuum dried before use. Oily sludge pyrolysis residues were sourced by pyrolyzing oily sludge from China's Xinjiang Kelamayi petrochemical factory.

Instruments used included a Tensor27 Fourier Transform Infrared Spectrophotometer (Bruker, Germany), a UV-2550 UV-Vis Spectrophotometer (Shimadzu, Japan), and a TECNAI-12 Transmission Electron Microscope (Philips, Netherlands).

Method of Preparing the Nano-adsorbent

A certain amount of supramolecular compounds TEOS, APS, and oily sludge pyrolysis residues were screened out to react with PTSC and Benzene Acylation Esters (BAE) forming intermediates.

Nanometer material TiO_2 was found to generate reactive ions on its surface by chemical modification. Nano-adsorbent NMA-12 may be created by reaction between the active hydroxyl and Benzene Acylation Esters by self-assembly of BAE on the surface of the nanometer material.

An electron microscopy photo of the nano-adsorbent NMA-12 is displayed in Figure 2. Nano-adsorbent NMA-12 is a type of spherical particle with an average diameter of approximately 250 nm.

RESULTS

Static Sorption Kinetics Curve

NMA-12 (0.2 g) samples were placed in 100 ml Erlenmeyer flasks and 50 mL of Congo red solution (phosphate buffer, 120 mg/L, pH 6.85) was added to each flask. Flasks were oscillated at 170 rpm at 25°C. Residual concentration of Congo red in the solution was measured by applying a UV-Vis absorption spectrum for a specific time interval until adsorption equi-
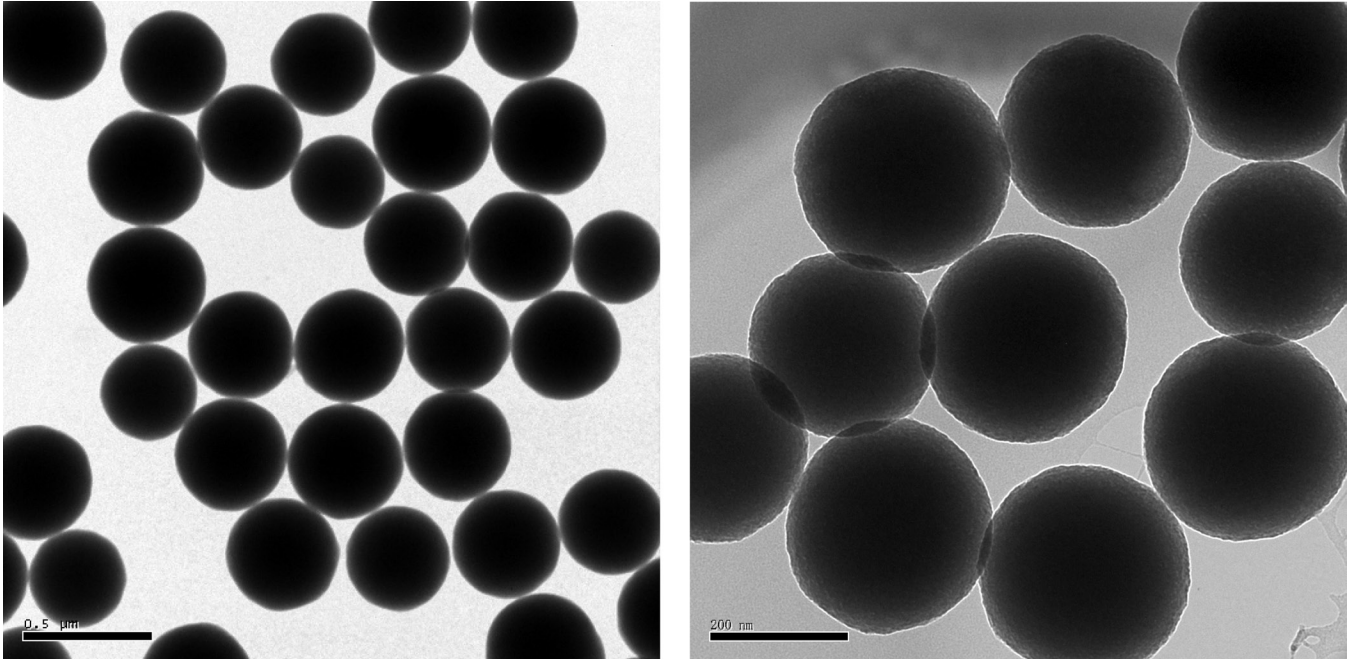
Figure 2. *Nano-adsorbent NMA-12 photos taken by transmission electron microscopy.*

librium was reached (See Figure 3) and converted to adsorbance (Q). By plotting Q against adsorption time the adsorption equilibrium time was determined to be approximately 150 minutes as displayed in Figure 4.

From the kinetics of adsorption formula, $-\ln(1 - Q_t/Q_\infty) = kt$, the adsorption reaction rate constant k may be obtained from the slope of a straight line of $\ln(1 - Q_t/Q_\infty)$ vs. t. Q_t and Q_∞ in the formula indicate reaction time and amount of Congo red adsorbed by each g of adsorbent at equilibrium, respectively. The appar-

ent rate constant of the adsorbent NMA-12 adsorbing Congo red is $k_{298} = 0.02$ s^{-1} from the slope of a straight line as displayed in Figure 5.

Adsorption Isotherms

Samples of adsorbent NMA-12 (0.1 g) were weighed and placed in 10 conical flasks with a volume of 100 mL per flask. Then, 50 mL of Congo red solution (phosphate buffer, pH = 6.85) at varying concentrations was placed within flasks. Samples were kept at 25°C and oscillated for 5 hours to reach adsorption equilibrium.

Figure 3. *UV-Vis absorption spectrum of Congo red solution with a certain amount of adsorbent NMA-12 at different adsorption times at 25°C (Adsorption time, t (curve 1–13): 0, 2, 5, 8, 15, 30, 50, 75, 100, 130, 150, 165, and 180 min).*
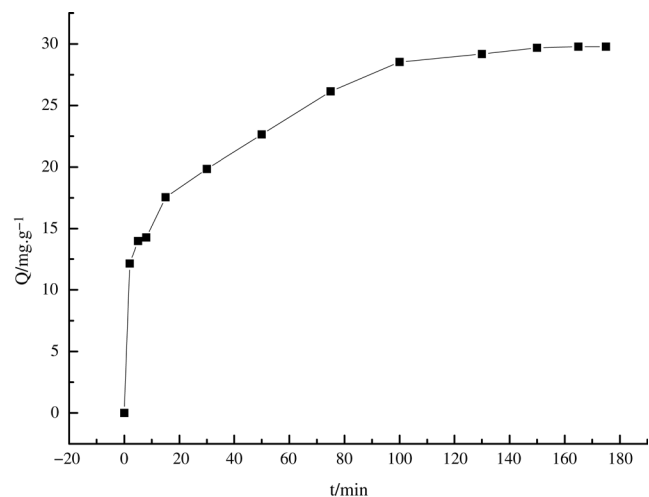
Figure 4. *Relationship between adsorbance and time (t).*
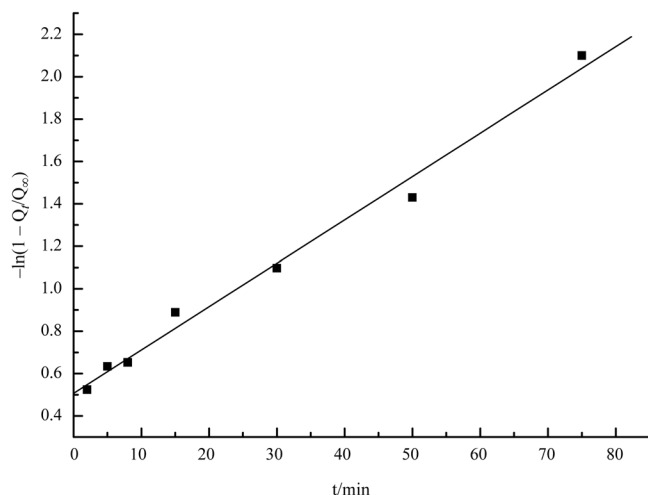
Figure 5. *Relationship between –ln(1 – Q_t/Q_∞) and time (t).*

Figure 6. *UV-Vis absorption spectrum of Congo red in the residual adsorption liquid at 25°C (Cinitial(mg/L): a. 40; b. 60; c. 80; d. 100; e. 120; f. 140; g. 160; h. 180; i. 200; j. 240.)*

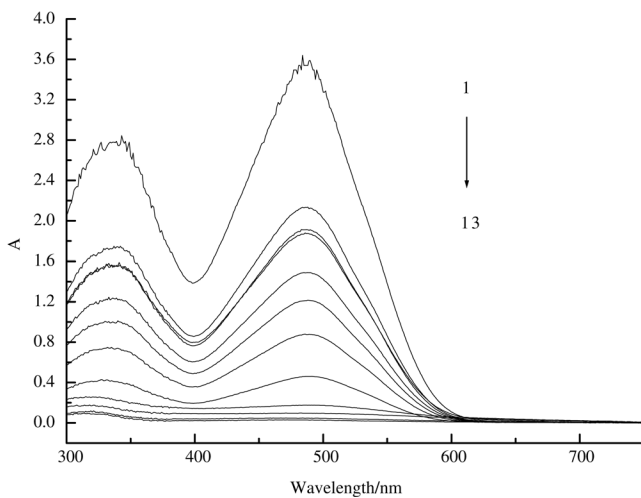Concentration of Congo red in the solution was measured by UV-Vis absorption spectroscopy at intervals until equilibrium was reached as seen in Figure 6.

Adsorbance, Q, was calculated and a plot relating Q and adsorbance time was created (See Figure 7). Maximum adsorbance of Congo red to adsorbent NMA-12 is 69.7 mg/g at 25°C.

When concentration of Congo red is lower than 5 mg/L the adsorbed quantity rises rapidly as concentration increases (See Figure 7). There is a different tendency when concentration of Congo red is higher than 5 mg/L. Adsorbed quantity approaches saturation value, 69.7 mg/g, asymptotically. Seen in Figure 6, it can be concluded that adsorption of Congo red to adsorbent NMA-12 follows a Langmuir adsorption model described by the following equation:

$$C^*/q = C^*/q_m + 1/Kq_m \qquad (1)$$

In this equation, C^* indicates concentration of Congo red (mg/L) in the solution at the adsorption equilibrium point and q and q_m are equilibrium adsorbance and maximum adsorbance (mg/g), respectively. Adsorption equilibrium constant is K. A plot of C^*/q against C^* yields the curve displayed in Figure 7. The linear relationship suggests that the adsorption processes conform well to the Langmuir adsorption model. Based on slope and intercept, maximum adsorption quantity q_m is 70.1 mg/g which is approximately equal to the experimentally derived value of 69.7 mg/g. The adsorption equilibrium constant, K, is 2.2 mg·L·g^{-2}.

Static Desorption Kinetics Characteristics Research

Samples of adsorbent NMA-12 (1.5 g) were ex-

posed to varying quantities of Congo red solution at 25°C under oscillation for 5 hours. Samples were filtered and dried at room temperature. Samples of the adsorbent NMA-12 (0.1 g) were weighed and put into 150 ml conical flasks with 50 mL of water and Congo red solution which contained Congo red at a concentration of 1×10^{-2} mol·L^{-1}. Flasks were oscillated at 25°C and Congo red residual concentration in solution was measured at fixed intervals until adsorption equilibrium was reached. Plotting the desorption concentration, c, of Congo red versus desorption time, t, results in a Congo red static desorption curve as seen in Figure 8. Initial desorption speed was slow while the quantity of Congo red desorbed from adsorbent increased significantly in either pure water or analytical liquid.
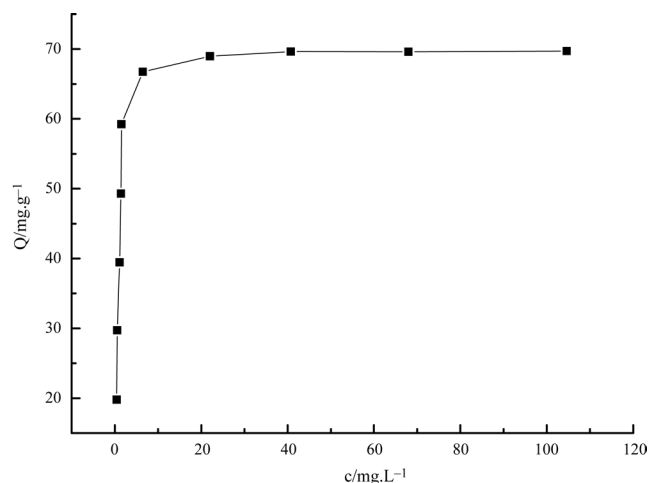
Figure 7. *Relationship between adsorbance and equilibrium concentration at 25°C.*
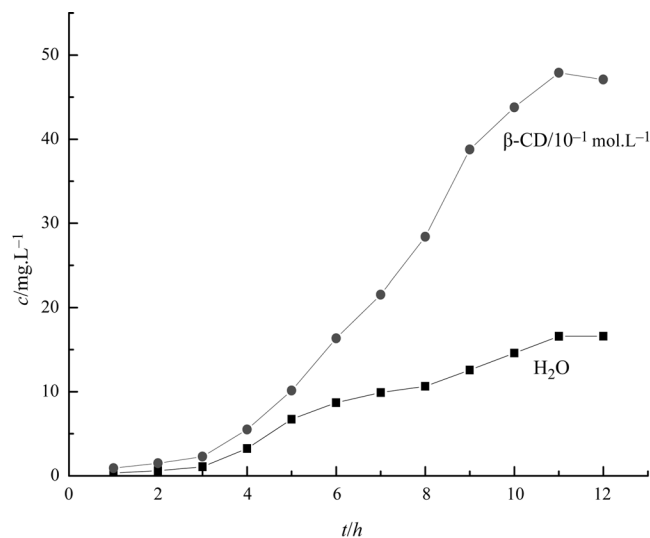
Figure 8. *Relationship between desorbed concentration and time (t).*

Solution reached maximum amount desorbed after 11 hours. Maximum desorption rate in pure water was approximately 30% and increased to 80.7% in analytical liquid. Amount of Congo red desorbing from the analytical agent would increase if concentration of analytical agent in the analytical liquid were increased.

CONCLUSIONS

There are three major items to conclude:

1. Benzene acylation ester was synthesized by reaction of the main synthetic monomers such as supermolecular compounds and oily sludge pyrolysis residues with PTSC. Benzene acylation ester was modified by nanometer materials and self-assembled on the surface of nanometer material. Nano-adsorbent NMA-12 was the product.

2. Using Congo red as the test adsorbate, static adsorption kinetics characteristics of adsorbent NMA-12 were studied and adsorption equilibrium time was approximately 150 minutes. The apparent rate constant of adsorption was $k_{298} = 0.02$ s^{-1}.

3. Static desorption kinetic characteristics of adsorbent NMA-12 were also investigated. Experimental results suggest initial desorption speed was slower while the desorbed quantity of Congo red

increased significantly over time regardless of pure water or analytical liquid as the reaction medium. The solution achieved maximum desorbed amount in 11 hours. Maximum desorption rate was approximately 30% in pure water and 80.7% in analytical liquid.

REFERENCES

1. Abouelnasr, A.M., and Zubaidy, E., "Treatment and Recovery of Oil-Based Sludge Using Solvent Extraction", SPE paper No. 118179, Abu Dhabi International Petroleum Exhibition and Conference, Abu Dhabi, UAE, 2008.

2. Brasquet, S.C., Coq, L.L., and Cloirec, P.L., "Structure Characterization and Adsorption Properties of Pyrolyzed Sewage Sludge", *Environmental Science & Technology,* Vol. 39, No.11, 2005, pp. 4249–4257.

3. Hahn, W.J., "High-Temperature Reprocessing of Petroleum Oily Sludges", SPE paper No. 25931, *SPE Production & Facilities,* Vol. 9, No.3, 1994, pp. 179–182.

4. Hahn, W.J., and Loehr, R.C., "Biological Treatment of Petroleum Oily Sludges", SPE paper No. 23997, Permian Basin Oil and Gas Recovery Conference, Midland, Texas, 1992.

5. Joseph, P. S., Philip, B. D., Michael, H.H., *et al.*, "Crude Oil Hydrocarbon Bioremediation and Soil Ecotoxicity Assessment", *Environmental Science & Technology,* Vol. 31, No.6, 1997, pp. 1769–1776.

6. Milne, B.J., Baheri, H.R., and Hill, G.A., "Composting of a Heavy Oil Refinery Sludge", *Environmental Progress,* Vol. 17, No. 1, 1998, pp. 24–27.

7. Nelson, O.R., Carlos, N. K., Lúcia, C.F., *et al.*, "ThermoChemical Process To Remove Sludge From Storage Tanks" SPE paper No. 105765, *SPE Projects, Facilities & Construction,* Vol. 4, No. 3, 2007, pp. 97–102.

8. Said, M., Elektorowicz, M., Ahmad, D., *et al.*, "A New Rapid Technique for Screening the Potential of Implanted Microorganisms to Tolerate and Grow on Petroleum Oily Sludges", *Environmental Technology,* Vol. 27, No. 10, 2006, pp. 1115–1123.

9. Seredych, M., and Bandosz, T. J., "Tobacco Waste/Industrial Sludge Based Desulfurization Adsorbents: Effect of Phase Interactions during Pyrolysis on Surface Activity", *Environmental Science & Technology,* Vol. 41, No. 10, 2007, pp. 3715–3721.

10. Jin, Y., Chen, M., Chen, K. P., *et al.*, "Pre-Caspian Basin Wells in Salt-Gypsum Beds Require an Optimized Drilling Fluid", *Oil & Gas Journal,* Vol. 108, No. 4, 2010, pp. 46–53.

11. Jin, Y., Chen, M., Chen, K. P., *et al.*, "Depressant Replaces Mechanical Method for Removing Blockage", *Oil & Gas Journal,* Vol. 107, No. 41, 2009, pp. 37–43.

Photocatalytic Degradation of Phenol-Containing Wastewater over Cu-Bi$_2$WO$_6$ Composite under Visible Light Irradiation

JING WANG, XIAOMING GAO, FENG FU*, LIPING ZHANG and YUFEI WU

Department of Chemistry and Chemical Engineering, Shaanxi Key Laboratory of Chemical Reaction Engineering, Yan'an University, Yan'an 716000, China

ABSTRACT: A semiconductor-based Cu-doped Bi$_2$WO$_6$ photocatalyst was synthesized successfully via the hydrothermal method. As-prepared samples were characterized by XRD, UV-vis DRS, SEM, and specific surface area. Results revealed that Cu-Bi$_2$WO$_6$ presented a structure of porous microspheres and a nanosheet as well as a crystal structure of orthorhombic phase. Photocatalytic properties were evaluated by degrading phenol-containing wastewater under visible light irradiation. Results showed that Cu-Bi$_2$WO$_6$ can display a more improved photocatalytic oxidative ability than pure Bi$_2$WO$_6$. Furthermore, the possible mechanism of photocatalysis has been addressed.

INTRODUCTION

THE problem that an aromatic fraction is not effectively degraded and is more poisonous in wastewater treatment has a serious influence on water quality. It had been confirmed that after it was induced by a light semiconductor, TiO$_2$ could be efficient in decomposing organic compounds [1]. Since then many studies about TiO$_2$ have been done in hopes of opening a new method for wastewater purification. However, the large band gap of TiO$_2$ makes it necessary for excitation only by UV light which limits usage efficiency of solar energy (max. 5%) and commercialization of this technology. Therefore, in order to eliminate the drawback the development of a new visible-light-driven photocatalyst has attracted greater attention.

Bismuth-oxide-based visible photocatalysts such as BiVO$_4$ [2–5], Bi$_2$WO$_6$ [6–8], and Bi$_2$MoO$_6$ [9–11] have recently drawn much interest because of their unique physical and chemical properties useful to photocatalytic oxidation. Understanding, Bi$_2$WO$_6$ a typical Aurivillius oxide structurally, related oxides with layer structure is a new hotspot for further study. It has been found to be effective to decompose organic dyes and contaminations under visible light radiation [12]. Much work has been carried out in order to enhance photocatalytic properties such as acid treatment

[7], calcining [8], ionic liquid-assisted hydrothermal method [13], and the hydrothermal method [14]. These methods could improve photocatalytic properties to some extent but cannot efficiently decrease photogenerated e^-/h^+ recombination rate. Recently, some reports have demonstrated that doping metal or nonmetal is a feasible method for eliminating the recombination rate of photogenerated e^-/h^+ and improving photocatalytic activity for instance for Ag-Bi$_2$WO$_6$ [15], C-Bi$_2$WO$_6$ [16], and AgBr-Ag-Bi$_2$WO$_6$ [17].

Considering synergetic effect between metal and semiconductor components in this study, Cu was loaded on Bi$_2$WO$_6$ to promote separation of the photogenerated electron-hole and to improve the photocatalysis. Cu-Bi$_2$WO$_6$ sample was prepared by hydrothermal method. Optical properties were characterized and photocatalytic activity of the Cu-Bi$_2$WO$_6$ sample was evaluated via photodegradation of phenol-containing wastewater under visible light irradiation. As an environment-friendly and economical oxidant, air was added into the photocatalytic reaction system with which the potocatalytic reaction effect can be promoted. A possible mechanism for phenol photocatalytic degradation over Cu-Bi$_2$WO$_6$ catalyst was also discussed.

EXPERIMENTAL

Preparation of Photocatalysts

All reagents were analytically "pure" and were

---

employed without any further purification. 10 mmol $Bi(NO_3)_3 \cdot 5H_2O$ was dissolved in 6 mL 15% nitric acid, 5 mmol $Na_2WO_4 \cdot 2H_2O$ was dissolved in 6 mL 15% Sodium hydroxide solution and then 0.002 g SDBS (sodium dodecyl benzene sulfonate) was added, respectively. After being stirred magnetically for 30 min the two solutions were mixed and mixture pH was adjusted by the acid/base solution above. Then, with an appropriate amount added (0.5%) $Cu(NO_3)_2$ the resulting solution was stirred for another 30 min. The yellowish precursor was sealed in a 25 mL Teflon liner stainless vessel which was heated to 140°C for 24 h. After the temperature slow-cooled from 140°C to 20°C the sample was filtered and washed using distilled water and absolute ethanol several times. Therefore, the yellow powder $Cu-Bi_2WO_6$ sample was obtained via drying at 80°C for 4 h.

Characterization of the Photocatalyst

$Cu-Bi_2WO_6$ was characterized with an X-ray diffractometer (XRD) by using monochromatized Cu Kα radiation under 40 kV (λ = 0.15418 nm) and 100 mA with the 2θ altering from 20º to 80º (Shimadzu 7000, Japan). Optical diffuse reflectance spectra of $Cu-Bi_2WO_6$ were obtained using a UV-vis spectrophotometer (Shimadzu UV-2550, Japan) with $BaSO_4$ as a reference and spectral range conversion from 200 to 800 nm. Morphologies and microstructures for samples were analyzed using a scanning electron microscope (SEM) (Hitachi TM3000, Japan). Specific surface area was analyzed by N_2 adsorption-desorption measurement (V-Sorb 2800P, China).

Photocatalytic Oxidative Degradation

Photocatalytic properties of $Cu-Bi_2WO_6$ samples were evaluated by degrading phenol-containing wastewater (concentration of phenol is 5 mg/L) at ambient temperature. A reaction solution of a suitable amount (0–2.0 g/L) of photocatalyst and phenol-containing wastewater were irradiated under a visible light source (i.e., metal halogen lamp, 400 w) and stirred magnetically. Meanwhile, a specific volume (10–35 mL/min) of dry air was blown into the reaction system. The reaction solution was centrifuged at a given time interval and phenol concentration was calculated by detecting absorbance using a UV-vis spectrophotometer. Degradation rate was calculated from percentage of phenol in wastewater before (c_0) and after (c_i) the photocatalytic oxidation reaction according to: $x = (c_0 - c_i)/c_0 \times 100\%$.

RESULTS AND DISCUSSION

XRD Patterns of $Cu-Bi_2WO_6$

XRD patterns for samples are provided in Figure 1. Sharp and obvious diffraction peaks show that samples are well crystallized and can be readily indexed to the orthorhombic phase of Bi_2WO_6 (JCPDS No.73-1126) which has characteristic diffraction peaks at 2θ = 28.24°, 32.77°, 47.04°, and 55.90°. Because of the small amount of Cu species content (0.5%) and high dispersion in samples no obvious diffraction peaks of the Cu species may be clearly detected in samples. However, a weak peak detected at 2θ = 35.5° maybe a CuO diffraction peak so it is deduced that for these tests CuO is present in the $Cu-Bi_2WO_6$ system [18]. Seen in Figure 1 with a variation of pH value from 1 to 7 intensity of diffraction peaks gradually strengthens. When pH value is altered to 9 diffraction peaks quickly weakened. This indicated an improperly synthesized environment.

UV-vis Spectra of $Cu-Bi_2WO_6$

The optical absorption property of a semiconductor material is determined by electronic structure and is relative to its photocatalytic activity [19]. UV-vis spectra samples are displayed in Figure 2. According to Figure 2, both Bi_2WO_6 and $Cu-Bi_2WO_6$ have absorption properties from the UV light region to visible light region. Fundamental absorption edge of Bi_2WO_6 was observed in a visible light region at about 440 nm indicating visible light absorption was due to intrinsic
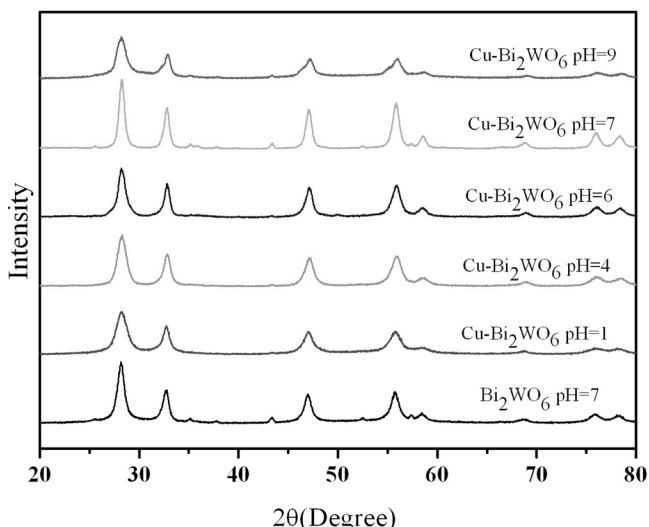
Figure 1. *XRD patterns of $Cu-Bi_2WO_6$ composite photocatalysts.*
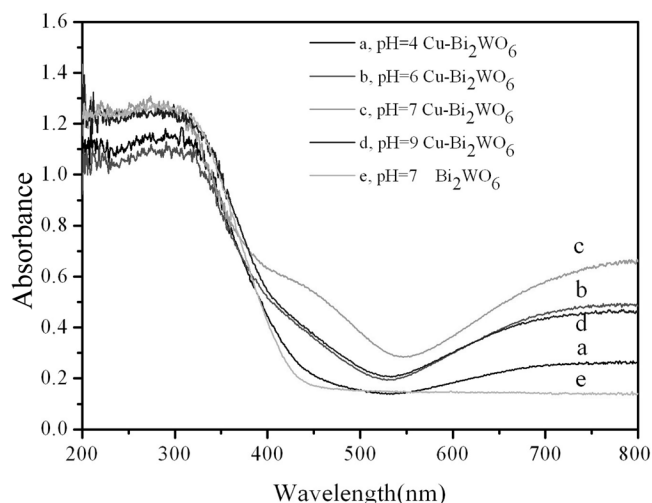
Figure 2. *UV-vis spectra of pure Bi$_2$WO$_6$ powders and Cu-Bi$_2$WO$_6$ powders.*

(a)

band-gap transition [20]. Considerable visible light absorption of Bi$_2$WO$_6$ is attributed to transition from the hybrid orbital of O 2p and Bi 6s to the W 5d orbital [21]. After Cu species doping, Cu-Bi$_2$WO$_6$ samples display a broader absorption edge than pure Bi$_2$WO$_6$. Absorption commences to enhance along with an increase of pH (1–7). These observed redshifts occurring after Cu species doping may be ascribed to a charge-transfer between metal ions and Bi$_2$WO$_6$ conduction band or valance band [18].

SEM Images of Cu-Bi$_2$WO$_6$

Light absorption and photochemical reaction take place on solid surfaces of photocatalysts. Thus, surface microstructure plays a key role in the photocatalytic process. Sample morphology and microstructure are displayed in Figure 3. Figure 3(a) shows SEM images of Cu-Bi$_2$WO$_6$ samples prepared at pH = 1 which appear as a homogeneous microspheres structure with average diameters of 3–4 μm. The high-magnification SEM image shows a rough surface and a porous structure for microspheres. Homogeneous nanosheet structure with an average size of 300 nm emerges when pH value was adjusted to 7 [See Figure 3(b)]. After pH value was adjusted to 9 as seen in Figure 3(c), the nanosheet became irregular and particle size increased to 1 μm. The aforementioned demonstrate that pH value plays a powerful role in crystal structure and microstructure.

Specific Surface Area Cu-Bi$_2$WO$_6$

Specific surface area is one of the key factors which

(b)

(c)
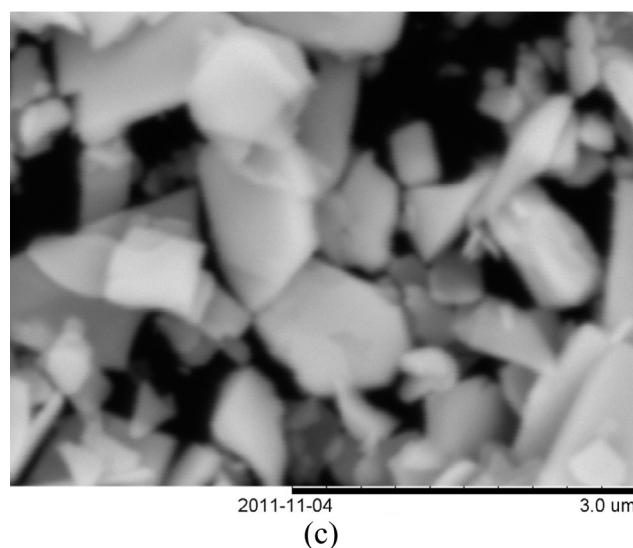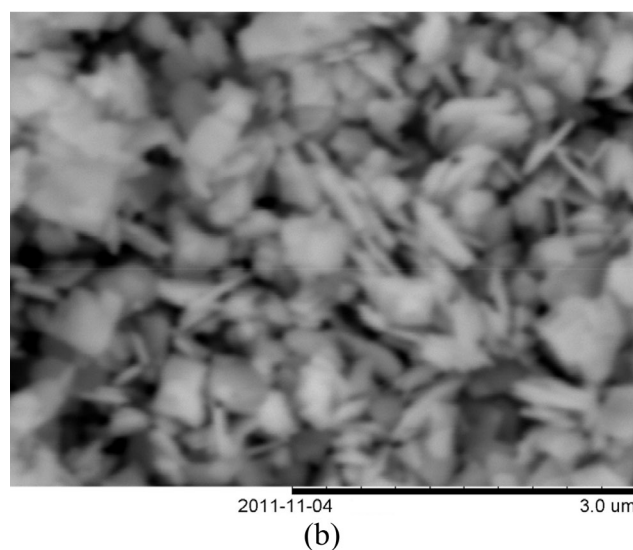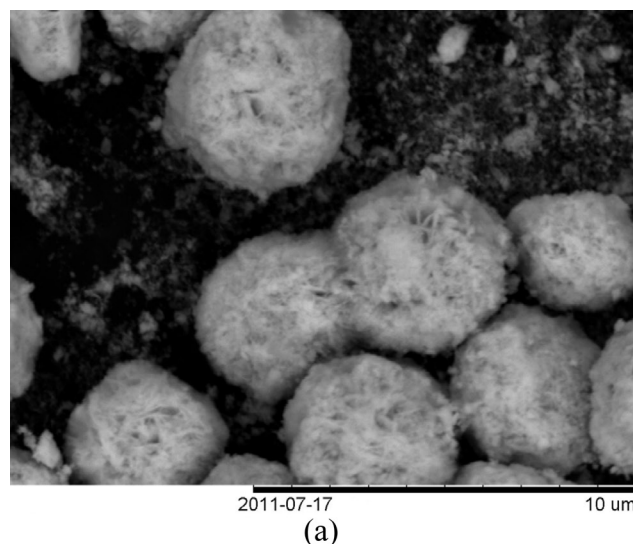
Figure 3. *SEM images of Cu-Bi$_2$WO$_6$ composite photocatalysts: (a) Cu-Bi$_2$WO$_6$ prepared at pH = 1, (b) Cu-Bi$_2$WO$_6$ prepared at pH=7, and (c) Cu-Bi$_2$WO$_6$ prepared at pH = 9.*

Table 1. Specifc Surface Area of Samples.

pH Value	Bi_2WO_6	$Cu-Bi_2WO_6$				
	6	1	4	6	7	9
BET Value (m^2/g)	30.895	31.624	37.733	43.473	47.114	34.733

effect catalyst abilities. Surface area values for the samples are displayed in Table 1. It is clear that specific surface area for all $Cu-Bi_2WO_6$ samples is larger than pure Bi_2WO_6 sample synthetized using the same method. BET surface area increases at first and then decreases with pH value for precursors changed from 1 to 9. The largest value is 47.114 m^2/g for a sample prepared at pH = 7.

PHOTOCATALYTIC OXIDATION PROPERTIES OF $Cu-Bi_2WO_6$

Influence of Different Prepared pH Value on Phenol Degradation

Figure 4 displays influence of different pH values for precursors on photocatalytic activity under visible light irradiation. It can be observed that with an irradiation time increase all samples exhibit increased degradation rate. During the beginning of the reaction O_2 was easily adsorbed on the catalyst surface and captured photoinduced electrons. Then, the phenol was oxidized by O_2 and photoinduced holes. Until 150 min the degradation rate tends to be stable. Maybe this is because a little polymeride was produced by some by-product degradation and polymeride blocked light transmission. In addition, $Cu-Bi_2WO_6$ demonstrates a higher degrada-

tion effect than pure Bi_2WO_6. Photodegradation of $Cu-Bi_2WO_6$ is weakened as precursors' pH is increased. This is mainly because $Cu-Bi_2WO_6$ crystallinity increases gradually while specific surface area quickly decreases. The latter led to a lower absorptive capacity of phenol on the surface of $Cu-Bi_2WO_6$ particles.

Effect of the Catalyst Amount on Phenol Degradation

Catalyst amount is an important factor in the application of a catalyst. Figure 5 displays the result of degradation rate variation with time in the presence of different catalyst amounts. According to Figure 5, with an increase of catalyst amount from 0 g/L to 1.5 g/L degradation rate exhibits a marked increase. There are two reasons. One is an increase of catalyst amount can promote absorptive performance between active centers of a catalyst surface to phenol and movement of electron-hole pairs of $Cu-Bi_2WO_6$. The other is an increase of catalyst amount may accelerate ·OH and O_2^- formation rate. However, when catalyst amounts are added to 2.0 g/L photodegradation is weakened. A reasonable explanation is that the catalytic particle may effect light transmittance of a solution causing higher light scattering and subsequently blocking light absorption by the catalyst.

Affect of Air Flow on Phenol Degradation

Appropriate addition of another oxidizing substance such as hydrogen peroxide (H_2O_2) into a photocatalytic oxidative system is a common means used to accelerate reaction. Figure 6 displays the result of degradation
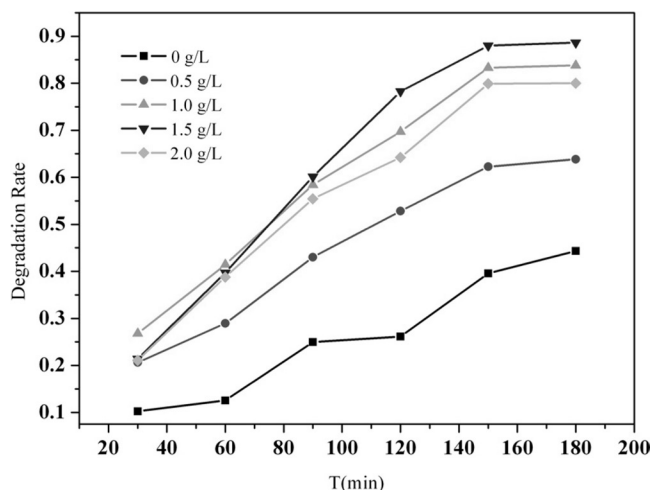

Figure 4. Influence of different prepared pH value on phenol degradation.

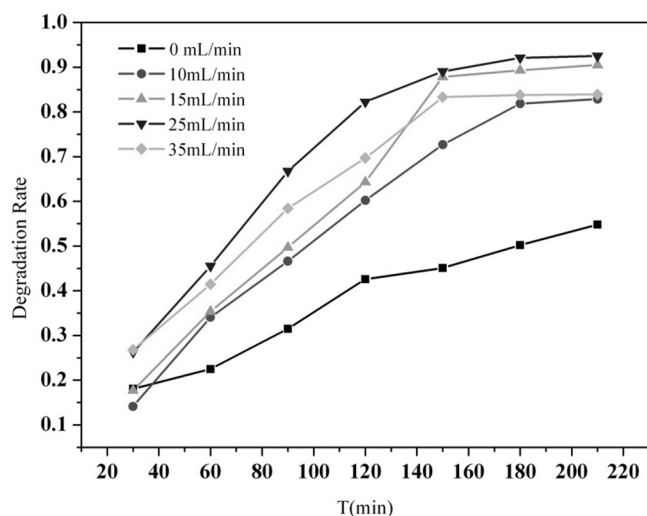**Figure 5.** Effect of catalyst amount on phenol degradation.

Figure 6. *Air flow effect on phenol degradation.*

rate variation with time under different air flow rates. Two sets of information may be observed. First, one is with irradiation time lasting until 150 min and tends to be stable. Degradation rate increases quickly. The other is with an increase of air flow from 10 mL/min to 35 mL/min. Degradation rate increases first and then decreases. The largest one is obtained under 25 mL/min. A possible explanation is that oxygen absorption on the photocatalyst surface is excited by visible light generating the superoxide ion O_2^- [22] and meanwhile decreasing e^-/h^+ recombination rate. The reaction was accelerated as a consequence of synergy between Cu-Bi₂WO₆ and O_2.

Recycling of Cu-Bi₂WO₆ Photocatalyst

Circulating runs were examined under operating condition (i.e., visible light irradiation, 1.0 mg/mL photocatalyst, 300 mL/min air flow) to confirm stability of high photocatalytic performance of Cu-Bi₂WO₆. Table 2 displays photodegradation results. The Photocatalyst exhibited strong catalytic ability in four previous recycling's although the photocatalytic property is slower than that of the first. This suggests a photocatalyst does not corrode in the photocatalytic oxidative process. This photocatalytic property decreases in the fifth recycling and could be due to agglomeration of catalyst particles in the recycling procedure.

Table 2. Recycling of Photocatalyst on Phenol Degradation.

Cycle-index	1	2	3	4	5
Degradation Rate	0.8330	0.8293	0.829	0.8197	0.6733

Mechanism Analysis of Photocatalytic Oxidation of Phenol

Photochemical oxidation and photocatalytic oxidation co-exist in the Cu-Bi₂WO₆ photocatalytic oxidative degradation process. Under visible light irradiation, Cu-Bi₂WO₆ absorbs photons of specific wavelength resulting in electrons in the valence band being excited to the conduction band meanwhile leaving charged holes in the valence band [Equation (1)] which is known as light-generated electrons (e^-) and hole (h^+):

$$Cu\text{-}Bi_2WO_6 + hv \rightarrow \\ Cu\text{-}Bi_2WO_6\,(h^+) + Cu\text{-}Bi_2WO_6\,(e^-) \tag{1}$$
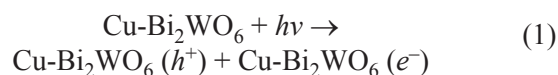
However, light-generated electrons (e^-) and hole (h^+) can easily recombine in bulk or on the surface of the semiconductor in the migration process leading to a marked decrease of photocatalytic reaction. A light-generated hole (h^+) may migrate to the surface to directly take part in oxidation reactions with phenol [Equation (2)] and also to react with H_2O molecules to form ·OH free radicals [Equation (3)] that may further oxidize phenol [Equation (4)].

$$Cu\text{-}Bi_2WO_6\,(h^+) + Phenol \rightarrow \\ Cu\text{-}Bi_2WO_6 + Phenol\ Oxidation\ Products \tag{2}$$

$$Cu\text{-}Bi_2WO_6(h^+) + H_2O \rightarrow H_2O + \cdot OH + H^+ \tag{3}$$

$$\cdot OH + Phenol \rightarrow Phenol\ Oxidation\ Products \tag{4}$$
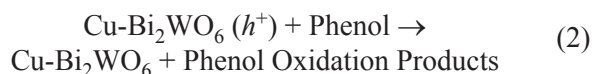
O_2 can capture light-generated electrons (e^-) and thus restrain recombination of electron-hole pairs effectively [23] and produce O_2^- [Equation (5)] non-selective strong oxidizing agents that react directly with the phenol molecule causing its degradation. [Equation (6)].

$$O_2 + Cu\text{-}Bi_2WO_6\,(e^-) \rightarrow Cu\text{-}Bi_2WO_6 + O_2^- \tag{5}$$

$$O_2^- + Phenol \rightarrow Oxidation\ products\ of\ Phenol \tag{6}$$
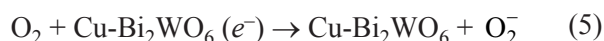
The degradation reaction was effectively enhanced regarding combined action of photochemical oxidation and photocatalytic oxidation.

CONCLUSIONS

A visible-light-driven photocatalyst, Cu-Bi₂WO₆, was successfully synthesized using a hydrothermal

method and characterized by conventional techniques. A photocatalytic property was evaluated to better understand photodegradation of phenol-containing wastewater. Results suggest the Cu-Bi_2WO_6 photocatalyst exhibited much higher photocatalytic oxidative ability than pure Bi_2WO_6. It is the desire of the authors this study may be helpful in the area of wastewater treatment.

ACKNOWLEDGEMENT

REFERENCES

1. T. Matsunaga, R. Tomada, T. Nakajima, H. Wake: "Photoelectrochemical sterilization of microbial cells by semiconductor powders", *FEMS Microbiol. Lett.* vol 29(1–2) (1985), p. 211–214.

2. S. Kohtani, J. Hiro, N. Yamamoto, A. Kudo, K. Tokumura, R. Nakagaki: "Adsorptive and photocatalytic properties of Ag-loaded $BiVO_4$ on the degradation of 4-*n*-alkylphenols under visible light irradiation", *Catal. Commun.,* vol 6(3) (2005), p. 185–189.

3. L. Zhou, W. Wang, S. Liu, L. Zhang, H. Xu, W. Zhu: "A sonochemical route to visible-light-driven high-activity $BiVO_4$ photocatalyst", *J. Mol. Catal. A: Chem.,* vol 252(1-2) (2006) p. 120–124.

4. X. Zhang, Z. Ai, F. Jia, L. Zhang, X. Fan, Z. Zou: "Selective synthesis and visible-light photocatalytic activities of $BiVO_4$ with different crystalline phases", *Mater. Chem. Phys.,* vol 103(1) (2007), p. 162–167.

5. L. Ge: J. Mol. Catal. A: "Novel visible-light-driven Pt/BiVO4 photocatalyst for efficient degradation of methyl orange", *Chem.,* vol 282(1-2) (2008), p. 62–66.

6. X. Zhao, Y. Wu, W. Q. Yao, Y. F. Zhu: "Photoelectrochemical properties of thin Bi_2WO_6", films *Thin Solid Films,* vol 515(11) (2007), p. 4753–4757.

7. G. Q. Zhang, N. Chang, D. Q. Han, A. Q. Zhou, X. H. Xu: "The enhanced visible light photocatalytic activity of nanosheet-like Bi_2WO_6 obtained by acid treatment for the degradation of rhodamine B", *Mater. Lett.,* vol 64(19)(2010), p. 2135–2137.

8. S. C. Zhang, C. Zhang, Y. Man, Y. F. Zhu: "Visible-light-driven photocatalyst of Bi_2WO_6 nanoparticles prepared via amorphous complex precursor and photocatalytic properties", *J. Solid State Chem.,* vol 179(1) (2006), P. 62–69.

9. Y. Shimodaira, H. Kato, H. Kobayashi, A. Kudo, "Photophysical properties and photocatalytic activities of bismuth molybdates under visible light irradiation", *J. Phys. Chem. B:* vol 110(36) (2006) 17790–17797.

10. Z. J. Zhang, W. D.Wang, M. Shang, W. Z. Yin: "Low-temperature combustion synthesis of Bi_2WO_6 nanoparticles as a visible-light-driven photocatalyst", *J. Hazard. Mater.,* vol 177(1-3) (2010), p. 1013–1018.

11. Y. Zheng, F. Duan, J. Wan, L. Liu, M. Q. Chen, Y. Xie: "Enhanced photocatalytic activity of bismuth molybdates with the preferentially exposed {010} surface under visible light irradiation", *J. Mol. Catal. A: Chem.,* vol 303(1-2)(2009), p. 9–14.

12. C. Zhang, Y. F. Zhu: "Synthesis of Square Bi_2WO_6 Nanoplates as High-Activity Visible-Light-Driven Photocatalysts", *Chem. Mater.* vol 17(13)(2005), p. 3537–3545.

13. J. X. Xia, H. M. Li, Z. J. Luo, H. Xu, K. Wang, S. Yin, Y. S. Yan: "Self-assembly and enhanced optical absorption of Bi_2WO_6 nests via ionic liquid-assisted hydrothermal method", *Mater. Chem. Phys.,* vol 121(1-2) (2010), p. 6–9.

14. H. B. Fu, W. Q. Yao, L. W. Zhang, Y. F. Zhang: "The enhanced photoactivity of nanosized Bi_2WO_6 catalyst for the degradation of 4-chlorophenol", *Mater. Res. Bull.,* vol 43(10) (2008), p.2617–2625.

15. J. Ren, W.Z. Wang, S.M. Sun, L. Zhang, J. Chang: "Enhanced photocatalytic activity of Bi_2WO_6 loaded with Ag nanoparticles under visible light irradiation", *Appl. Catal. B: Environ.,* vol 92(1-2) (2009), p. 50–55.

16. Y. L. Chen, X. X. Cao, J. D. Kuang, Z. Chen, J. L. Chen, B. Z. Lin: "The gas-phase photocatalytic mineralization of benzene over visible-light driven Bi_2WO_6@C microspheres", *Catal. Commun.,* vol 12(4)(2010), p. 247–250.

17. L. S. Zhang, K. H. Wong, Z. G. Chen, J. C. Yu, J. C. Zhao, et al.: "AgBr-Ag-Bi_2WO_6 nanojunction system: A novel and efficient photocatalyst with double visible-light active components", *Appl. Catal. A: Gen.,* vol 363(1-2) (2009), p. 221–229.

18. H. Xu, H. M. Li, C. D. Wu, *et al.*: "Preparation, characterization and photocatalytic properties of Cu-loaded $BiVO_4$", *J. Hazard. Mater.,* vol 153(1-2) (2008), p. 877–884.

19. X. F. Zhang, X. Quan, S. Chen, Y.B. Zhang: "Effect of Si doping on photoelectrocatalytic decomposition of phenol of $BiVO_4$ film under visible light", *J. Hazard. Mater.,* vol 177 (1-3) (2010), p. 914–917.

20. A. Kudo, I. Tsuji, H. Kato, "$AgInZn_7S_9$ solid solution photocatalyst for H_2 evolution fromaqueous solutions under visible light irradiation", *Chem. Commun.* Vol 38(17) (2002) 1958–1959.

21. Q. Xiao, J. Zhang, C. Xiao, X. K. Tan: "Photocatalytic degradation of methylene blue over Co_3O_4/Bi_2WO_6 composite under visible light irradiation", *Catal. Commun.,* vol (6)(2008), p. 1247–1253.

22. S. Tokunaga, H. Kato, A. Kudo:"Selective Preparation of Monoclinic and Tetragonal $BiVO_4$ with Scheelite Structure and Their Photocatalytic Properties", *Chem. Mater.,* vol 13(12) (2001), p. 4624–4628.

23. M. Shang, W. Z. Wang, S. M. Sun, J. Ren, L. Zhou, L. Zhang:" Preparation of monoclinic $BiVO_4$ thin film by citrate route for photocatalytic application under visible light", *J. Phys. Chem. C:* vol 1139(47) (2009), p. 20228–20233.

Effect of Different Aeration Rates on the Composting Process and Its Enzymatic Activities

Z. XU[1], L. L. ZHANG[2] and J. LI[2],*

[1]College of Resources and Environmental Science, Yunnan Agricultural University, Kunming 650201, China.

[2]College of Resources and Environmental Science, China Agricultural University, Beijing 100193, China

ABSTRACT: A pilot experiment was carried out to investigate effects of different aeration rates (A: 0.01, B: 0.02, C: 0.03, and D: 0.04 $m^{-3} \cdot min^{-1}$) on decomposition of organic waste and enzymatic activities during the composting process in a 100L bioreactor. Compared with lower aeration rates (A and B), higher aeration rates (C and D) could effectively improve the composting process in terms of promoting temperature and oxygen consumption, lowering C/N ratio, and significantly increasing all enzyme activities including those for protease, urease, dehydrogenase, β-glucosidase, and cellulase during the composting period.

INTRODUCTION

CHINA is a large agricultural country with large quantities of organic solid wastes generated every year. Annual production of animal manure, municipal solid waste, and sewage sludge were around 2,400, 160, and 14 million tons. Most organic solid wastes were discarded without any treatment and wastes had been considered a main non-point source form of pollution on farmland and in water bodies [29].

Composting was an important method regarding conversion of organic solid wastes into organic fertilizer which may increase concentration of organic matter in the soil. Enzymes released by microorganisms during composting break down complex organic compounds into simple water soluble material [5]. Numerous studies have shown major active enzymes involved in the composting process include: cellulases, β-glucosidases, proteases, urease, and dehydrogenase [4,6,19]. There were significant correlations between those enzymatic activities [6] and the composting process such as that of Castaldi *et al.* (2008) who found that hydrolase (protease, urease, cellulase, and b-glucosidase) and dehydrogenase activities were an increase of easily decomposable organic compounds in maturation phase [6]. Enzymatic activities tended to gently decrease suggesting stabilization of organic matter. A high correlation among all enzyme activities and between each activity and water-soluble carbon (WSC) led to a conclusion that both hydrolytic and dehydrogenase activities could be feasible indicators of state and evolution of organic matter [5]. Quantifying and characterizing enzymatic activities during composting may reflect the dynamics of the composting process in terms of decomposition of organic matter and nitrogen transformations. It may also provide information about maturity of composted products [25]. Enzymatic activity determination in contrast to most analytical techniques used for compost stability evaluation was easy, fast, and relatively expensive [19].

Aeration rate is considered to be the most important factor influencing successful composting [10]. Insufficient aeration (i.e., low aeration rate) may facilitate anaerobic conditions due to lack of oxygen. Pagans *et al.* (2006) reported that limiting oxygen decreased biodegradability [20] while excessive aeration may increase costs and slow down the composting process via heat, water, and ammonia losses [12]. Time-continuous or intermittent ventilation were chosen. Studies have shown that different ventilation modes, composting of raw materials, and rate of aeration is not the same (e.g, $0.25 \ L \cdot min^{-1} \cdot kg^{-1}$ volatile solids [ventilation method is continuous aeration and raw material is dairy manure with rice straw] [15], $0.1 \ m^3 \cdot min^{-1} \cdot m^{-3}$ [ventilation method is intermittent aeration of 30 min on/30 min off and raw material is chicken manure with straw and dry grasses] [24], and $0.4 \ L \cdot min^{-1} \cdot kg^{-1}$ organic matter [ventilation method is intermittent aeration of 15 min on/45 min off and raw material is grass, tomato, pepper

*Author to whom correspondence should be addressed.
E-mail: ceup_si@163.com

and eggplant wastes]) [14]. Adequate and appropriate aeration is an important factor effecting compost temperature variation, improvement of aerobic microbial activities and enzymatic activities [21,27], and further decomposition of organic wastes [8,23].

Changes of temperature, oxygen concentration, and enzyme activities under four different aeration rates during composting were investigated. The aim was to explain a relationship between various indicators and optimal aeration mode. Furthermore, this provides a basic parameter of forced aeration for rapid composting.

MATERIALS AND METHODS

Experimental Materials

Mixtures of air-dried chicken manure, fresh furfural residue, and dry bagasse in the ratio of 4:4:1 (w.w./w.w.) were used. Chicken manure was from a farm owned by the China Agriculture University in Beijing, China. Furfural residue and bagasse were purchased from a sugar factory in Gaocheng, Hebei province, China. C/N ratio and moisture content of the mixtures were adjusted to 30% and 55%, respectively. Properties for raw materials are displayed in Table 1.

Experimental Design

Basic Aeration Rate Determination

Total weight of materials was 50 kg and about 50% of materials were assumed to be degradable. 25% was degraded after the first phase. Meanwhile, moisture was reduced by 45%. It had been calculated that total aeration was 108.34 kg of which biochemical aeration was 12.93 kg and moisture elimination aeration was 95.41 kg [7]. The time of the first fermentation phase was 15 days and the air blower switching time was in a proportion of 1:5 (opening/closing). According to these aforementioned assumptions, basic aeration rate was set as 0.02 $m^3 \cdot min^{-1}$ (4.82 kg air$\cdot kg^{-1}$ dry matter).

Composting Set-up

A mixture (50 kg) was thoroughly mixed as a homogeneous feedstock into a horizontal and cylindrical reactor of 48 cm inner diameter and 56 cm length. Figure 1 provides a display of the structure of the experimental reactor. An "S" shaped pipeline was welded at the bottom of the fermentation tank and along the pipeline gas was pumped through a series of holes (1 mm diameter) located at 80 mm intervals.

According to the basic aeration rate of 0.02 $m^3 \cdot min^{-1}$ (4.82 kg air$\cdot kg^{-1}$ dry matter), the experiment contained 4 treatments as follows: 0.01 $m^3 \cdot min^{-1}$ (A, 2.41 kg air$\cdot kg^{-1}$ dry matter), 0.02 $m^3 \cdot min^{-1}$ (B, CK, 4.82 kg air$\cdot kg^{-1}$ dry matter), 0.03 $m^3 \cdot min^{-1}$ (C, 7.23 kg air$\cdot kg^{-1}$ dry matter) and 0.04 $m^3 \cdot min^{-1}$ (D, 9.64 kg air$\cdot kg^{-1}$ dry matter). Aeration frequency was at half-hour intervals after six minutes of aeration. The experiment was continually operated for 15 days from January 21 to February 6, 2008. Composting material was turned over once every 7 days. Samples were taken every 3 days and five sub-samples of composting material (about 500 g each) were taken from each reactor on days 0, 3, 6, 9, 12, and 15 and thoroughly mixed. Each sample was divided up into two samples, an air-dry and a fresh. The air-dried sample was prepared for chemical analysis and the fresh sample was stored at 4°C in a refrigerator for enzyme activities analysis.

Analytical Methods

Physico-chemical Analysis

Temperature and oxygen concentration were measured using thermal probes (PT100 sensor, Beijing Sailing Tech. Co., Ltd., China) and an oxygen sen-

Table 1. Properties of Raw Materials.

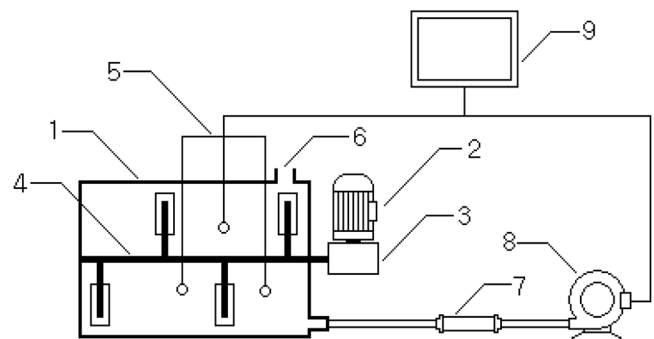| Materials	Materials Moisture Content (%)	TOC (g/kg)	TN (g/kg)	C/N (−)
Air-dried chicken manure	17.2	180	15	12
Furfural residue	46.1	350	10	35
Bagasse	41.7	468	12	39

Figure 1. Schematic of the experimental reactor. (1) Fermentation vessel, (2) Electromotor, (3) Reducer, (4) Churn-dasher, (5) Probes, (6) Exhausted gas, (7) Flow meter, (8) Ventilator, and (9) Computer monitoring.

sor (GNL-8100, Shanghai Chang'ai Electronic Sci. & Tech. Co., Ltd., China). The values of temperature and oxygen concentration were automatically recorded on-line every 10 minutes. Organic carbon content and total nitrogen (N-Kjedahl) were determined according to standard procedures [3]. Concentration of water-soluble carbon (WSC) was determined by oxidation with potassium dichromate [9].

Enzymatic Activity Assays

Samples of enzymatic activity assays were fresh and sieved (< 2 mm). Activities of protease, urease, and dehydrogenase were measured according to Alef and Nannipieri (1995) [2]. Procedures for evaluating cellulase activity was taken from Li *et al.* (2008) [15].

Statistical Analysis

Statistical analysis of data was carried out using SPSS 11.5 for windows. One-way analysis of variance (ANOVA) was used to compare mean values from different treatments (LSD, $P < 0.05$). Bivariate correlation was used to analyze relationships among various indicators.

RESULTS AND DISCUSSION

Temperature and Oxygen Concentration Changes

Effect of different aeration rates on composting temperature is displayed in Figure 2(a). The experiment was conducted in spring with an ambient extra ventricular temperature below 5°C and room temperature at about 10°C. Temperatures of treatment C and D were increased above 50°C after four days of composting and average growth rates of temperature were 0.76°C·h^{-1} and 0.8°C·h^{-1}, respectively. On other hand, 6 days and 5 days were needed for treatment A and B to get temperatures above 50°C. Average growth rates of temperature were only 0.53°C·h^{-1} and 0.66°C·h^{-1}, respectively. The thermophilic phase (> 50°C) of treatment A, B, C, and D were 5.0, 5.2, 5.9, and 6.2 days, respectively. The highest temperature of treatment A, B, C, and D were 58.5, 57.5, 60.5, and 64.5°C, respectively. Results suggest that a higher aeration rate (C and D) could effectively improve the composting process compared with the lower aeration rates of A and B.

Changes of oxygen concentration during composting are displayed in Figure 2(b). Oxygen concentrations for all treatments had no differences for the first

Figure 2. *Changes of temperature and oxygen concentration during composting (A: 0.01 m³·min⁻¹, 2.41 kg air·kg⁻¹ dry matter; B: 0.02 m³·min⁻¹, 4.82 kg air·kg⁻¹ dry matter; C: 0.03 m³·min⁻¹, 7.23 kg air·kg⁻¹ dry matter; D: 0.04 m³·min⁻¹, 9.64 kg air·kg⁻¹ dry matter).*

two days. Oxygen consumption started to increase and oxygen concentration of the pile reduced markedly within 4–9 days of thermophilic phase. Oxygen concentrations in the pile were increased at the later stages of 10~15 days. During the entire process of composting, oxygen concentration in the piles was maintained from 8 to 20%. However, treatments with a higher aeration rate (C and D) could maintain a higher degree of oxygen concentration than that of lower aeration rates (A and B) during periods of high temperature.

Aeration rate effected rate of raising temperature during composting. Conversely, the temperature of composting effected oxygen concentration in piles and there was a very significant negative correlation observed between temperature and oxygen concentration ($r = -0.918$, $p < 0.01$).

C/N Ratio and Water-Soluble Carbon (WSC)

C/N ratio is a proper index used to evaluate compost maturity. Changes in C/N ratios were a result of changes in nitrogen contents and organic matter. As seen in Figure 3(a), C/N ratio for all treatments gradually declined from 29 to around 20 at the end of 15 days of composting. Especially, C/N was reduced more rapidly in higher aeration rate treatments for C (20) and D (18.9). This decline was due to the formation and loss of CO_2 [13]. Raut *et al.* (2008) also suggested a C/N ratio below 20 is indicative of acceptable compost maturity that during efficient composting is obtained due to degradation of organic matter [21]. However, treatment C and D were not significantly different (p < 0.05) for day 15.

Water-soluble carbon (WSC) was one of the readily biologically active parameters effecting compost sta-

bility [6,17]. WSC concentrations decreased gradually during the composting process for all treatments of A, B, C, and D. Figure 3(b) also displays degradation of soluble organic carbon for all treatments during 6–12 days of composting. Therefore, it showed that a higher aeration rate promoted decomposition of organic matter and benefited the process of composting.

Enzyme Activities

Protease activity was closely related to the nitrogen cycle and catalyzes the hydrolysis of proteins to ammonia while acting on short-chain poly peptide substrates. Liu *et al.* (2011) also reported protease is an important enzyme and considered as an appropriate indicator of organic matter decomposition during composting [17].

During the beginning days of the in-vessel composting process protease activity was increased for all treatments [See Figure 4(a)]. Enzymes were decreased gradually up to 15 days of treatment after three days of composting. Initial increase of protease may be due to availability of polypeptides in the initial mixture. It was interesting that a higher aeration ratio benefited protease activity during an earlier stage of composting (0–3 days) with a peak order of D > C >B >A. Aira *et al.* (2007) suggested protease activity is highly dependent on substrate availability. Here, the decline of protease at end of the composting process is demonstrated [1].

Changes of urease activity were similar to those of protease [See Figure 4(b)]. Among the different aeration treatments urease activity was higher for treatment D and C than for B and A. Urease activity increased at the beginning of composting most likely due to a high degree of substrate availability [11]. Also, urease activity was closely related to the nitrogen cycle since it is related to hydrolysis of urea to ammonium and carbon dioxide.

Figure 4(c) displays changes in dehydrogenase activity during composting. Mokhtari *et al.* (2011) suggested the dehydrogenase enzyme was produced as a result of microbial activity [18]. Xiao and Zeng (2009) found dehydrogenase enzyme activity increases rapidly from 0.75 to 3.42 mg Triphenylformazan (TPF)/g. day in the early days of composting and then a decreasing trend starts that finally reaches 0.45 mg TPF/g.day at the end of the cooling (mesophilic) phase [29]. It was discovered that dehydrogenase activity increased rapidly up to 6 days and hits the peak at high-temperature stage. Then, it decreased gradually. Xiao and Zeng (2009) also found a similar pattern of initial increases and final decreases of dehydrogenase activity for the

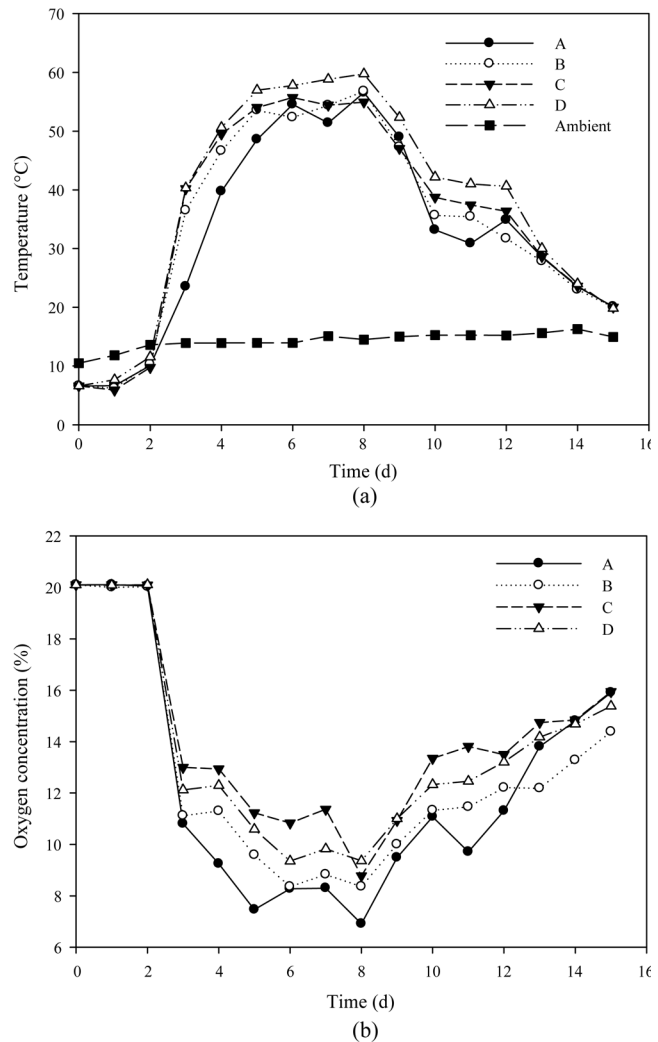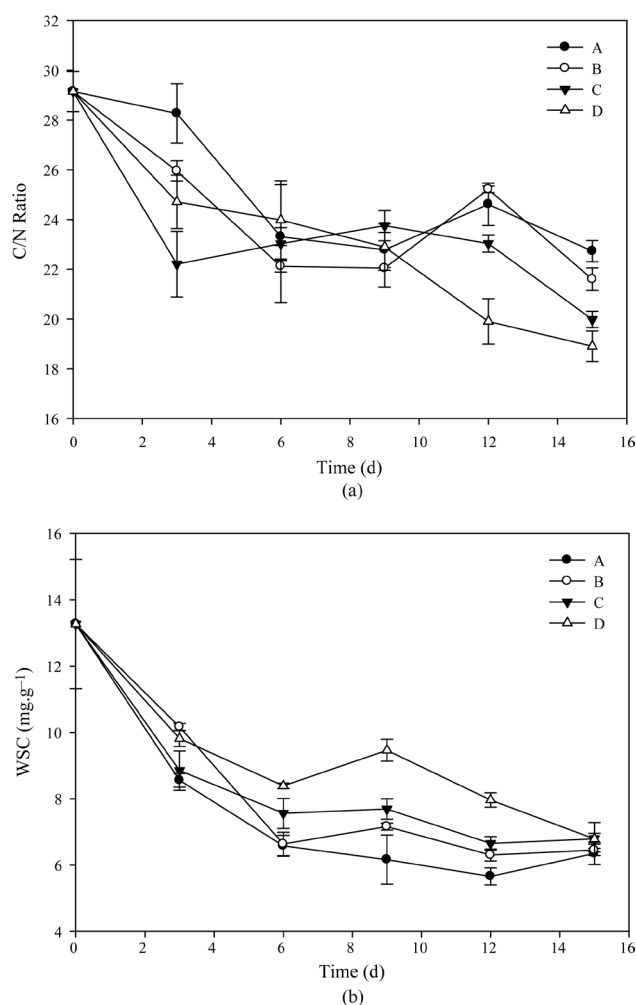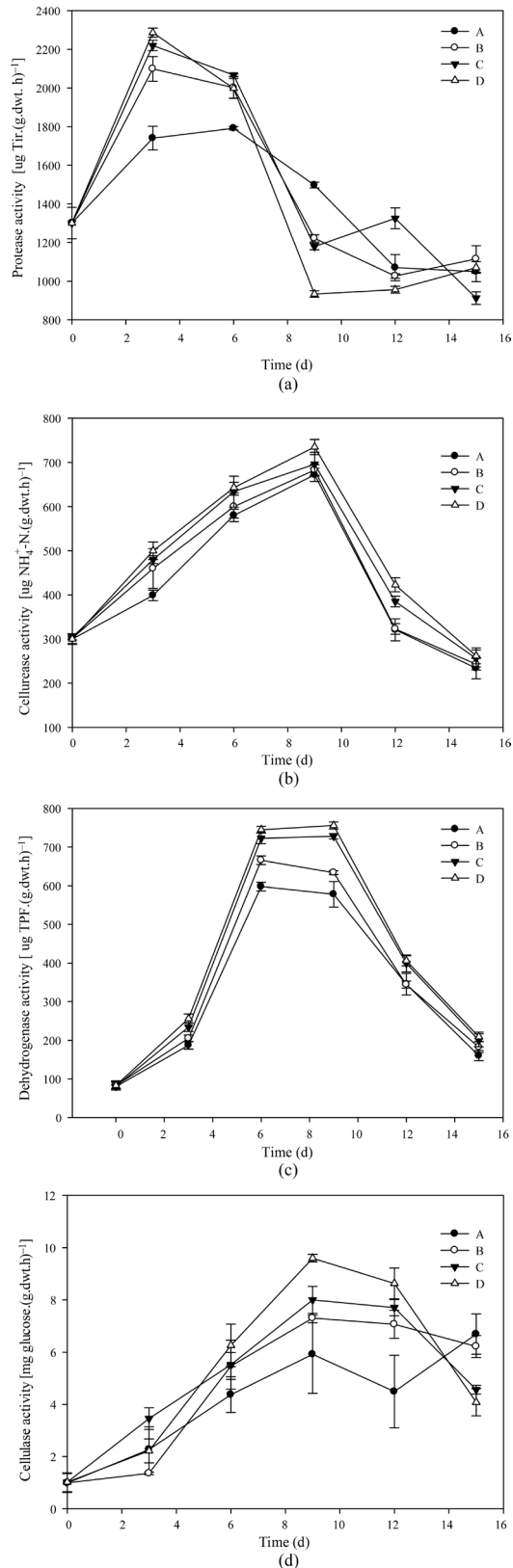*Figure 3. Changes of C/N ratio and WSC during composting (A: 0.01 m³·min⁻¹, 2.41kg air·kg⁻¹ dry matter; B: 0.02 m³·min⁻¹, 4.82 kg air·kg⁻¹ dry matter; C: 0.03 m³·min⁻¹, 7.23 kg air·kg⁻¹ dry matter; D: 0.04 m³·min⁻¹, 9.64 kg air·kg⁻¹ dry matter).*

Figure 4. *Changes of (a) protease activity, (b) urease activity, (c) dehydrogenase activity, and (d) cellulase activity during composting (A: 0.01 m³·min⁻¹, 2.41kg air· kg⁻¹ dry matter; B: 0.02 m³·min⁻¹, 4.82 kg air· kg⁻¹ dry matter; C: 0.03 m³·min⁻¹, 7.23 kg air·kg⁻¹ dry matter; D: 0.04 m³·min⁻¹, 9.64 kg air· kg⁻¹ dry matter)*

in- vessel composting process [29]. Dehydrogenase activity for treatments D and C were significantly higher than for treatments A and B ($p < 0.05$). Dehydrogenase activity for treatment B was also higher than for treatment A but there were no significant differences between treatments C and D ($p < 0.05$). Since dehydrogenase was involved in respiratory chains for all microorganisms its activity was used as a measure of overall microbial activity [22]. Dehydrogenase activity was negatively correlated with oxygen concentration and positively correlated with temperature similar to those of Barrena (2008) [4]. Dehydrogenase activity was correlated with urease activity ($r = 0.892$, $p < 0.01$) and cellulase activity ($r = 0.695$, $p < 0.01$).

Figure 4(d) displays cellulase activity for different aeration experiments. Results suggest that cellulose activity increased in the first 9 days and then was followed by a decline in accordance with the findings of Raut *et al.* (2008) [21]. However, cellulase activity increased again during the cooling phase. During the high-temperature period, cellulase activity for treatment D was significantly higher than that for other treatments ($p < 0.05$). Cellulase activity for treatment A was the lowest and there were no significant differences between treatments B and C ($p < 0.05$). Finally, cellulase activity was correlated with temperature ($r = 0.608$, $p < 0.01$), WSC ($r = 0.507$, $p < 0.05$).

CONCLUSIONS

Treatment using a basic aeration rate (0.02 m³·min⁻¹, 4.82 kg air· kg⁻¹ dry matter) was able to complete the composting process. It was appropriate to increase aeration (i.e., 0.03 or 0.04 m³·min⁻¹, 7.23 or 9.64 kg air· kg⁻¹ dry matter). It was more advantageous to raise temperature, maintain concentration of oxygen in the pile, decrease C/N, and promote aerobic activity for the in-vessel composting process.

Regarding treatments with an aeration rate of 0.03–0.04 m³·min⁻¹ (7.23–9.64 kg air·kg⁻¹ dry matter), it was observed that notable enzyme activity increased with protease, urease, dehydrogenase, and cellulase during the earlier stages of composting as compared with those with a rate of 0.02 m³·min⁻¹ or less. This reflects the fact that appropriately increasing aeration rate could promote the process of aerobic composting. The aeration rate (0.02 m³·min⁻¹, 4.82 kg air·kg⁻¹dry matter) was used to meet the basic needs of the composting process. Aeration rates of 0.03–0.04 m³·min⁻¹ (7.23–9.64 kg air·kg⁻¹ dry matter) were more helpful for carrying out the composting process.

ACKNOWLEDGMENTS

REFERENCES

1. Aira, M., Monroy, F., Domínguez, J., "Earthworms strongly modify microbial biomass and activity triggering enzymatic activities during vermicomposting independently of the application rates of pig slurry", *Sci. Total Environ.,* Vol. 385, No.1–3, 2007, pp. 252–261.

2. Alef, K., Nannipieri, P., 1995. Methods in applied soil microbiology and biochemistry, Academic Press, London.

3. Bao, S. D., 2000. Soil and agricultural chemistry analysis, 3rd Ed. China Agriculture Press, Beijing.

4. Barrena, R., Vázquez, F., Sánchez, A., "Dehydrogenase activity as a method for monitoring the composting process", *Biores. Technol.,* Vol.99, No. 4, 2008, pp. 905–908.

5. Benitez, E., Nogales, R., Elvira, C., Masciandaro, G., Ceccanti, B., "Enzyme activities as indicators of the stabilization of sewage sludges composting with eisenia foetida", *Biores. Technol.,* Vol.67, No. 3, 1999, pp. 297–303.

6. Castaldi, P., Garau, G., Melis, P., "Maturity assessment of compost from municipal solid waste through the study of enzyme activities and water-soluble fractions", *Waste Manage.,* Vol.28, No. 3, 2008, pp. 534–540.

7. Cai, J. C., 1990. "Compost project and compost factory", Mechanical industry publishing house, Beijing.

8. Chang, Q. X., Wei, Y. S., Liu, J. X., "Changes of nitrogen and phosphorus in animal manure composting with different aeration control modes", *Acta Scientiae Circumstantiae,* Vol.27, No. 5, 2007, pp. 732–738.

9. Ciavatta, C., Govi, M., Vittori, A. L., Sequi, P., "Characterization of humified compounds by extraction and fractionation on solid polyvinylpyrrolidone", *J. Chromatogr. A,* Vol. 509, No. 1, 1990, pp. 141–146.

10. Diaz, M. J., Madejon, E., Lopez, F., Lopez, R., Cabrera, F., "Optimization of the rate vinasse/grape marc for co-composting process", *Process Biochem.,* Vol.37, No.10, 2002, 1143–1150.

11. Garcia, C., Hernandez, T., Costa, F., Ayuso, M., "Evaluation of maturity of municipal waste compost using simple chemical parameters", *Commu. Soil Sci. Plant Anal.,* Vol.23, No.13&14, 1992, pp. 1501–1512.

12. Guo, R., Li, G. X., Jiang, T., Schuchardt, F., Chen, T. B., Zhao, Y., Shen, Y. J., "Effect of aeration rate, C/N ratio and moisture content on the stability and maturity of compost", *Biores. Technol.,* Vol.112, No. 5, 2012, 171–178.

13. Haroun, M., Idris, A., Syed Omar, S. R.,"A study of heavy metals and their fate in the composting of tannery sludge", *Waste Manage.,* Vol.27, No.11, 2007, pp. 1541–1550.

14. Kulcu, R., Yaldiz, O., "Determination of aeration rate and kinetics of composting some agricultural wastes". *Biores. Technol.,* Vol. 93, No.1, 2004, pp. 49–57.

15. Li, M., Peng, X. Y., Zhao, Y. C., Ding, W. C, Cai, H. S, Liu, G. T, Wu, Z. S, "Microbial inoculum with leachate recirculated cultivation for the enhancement of OFMSW composting", *J. Hazard. Mater.,* Vol.153, No.2, 2008, pp. 885–891.

16. Li, X., Zhang, R., Pang, Y., "Characteristics of dairy manure composting with rice straw", *Biores. Technol.,* Vol. 99, No.2, 2008, pp. 359–367.

17. Liu, D., Zhang, R., Wu, H., Xu, D., Tang, Z., Yu, G., Xu, Z., Shen, Q., "Changes in biochemical and microbiological parameters during the period of rapid composting of dairy manure with rice chaff", *Biores. Technol.,* Vol.102, No.19, 2011, pp. 9040–9049.

18. Mokhtari, M., Nikaeen, M., Amin, M. M., Bina, B., Hasanzadeh, A., "Evaluation of stability parameters in in- vessel composting of municipal solid waste", *Iran. J. Environ. Health. Sci. Eng.,* Vol. 8, No.4, 2011, pp. 325–332.

19. Mondini, C., Fornasier, F., Sinicco, T., "Enzymatic activity as a parameter for the characterization of the composting process", *Soil Biol. Biochem.,* Vol.36, No.10, 2004, pp. 1587–1594.

20. Pagans, E., Barrena, R., Font, X., Sánchez, A., "Ammonia emissions from the composting of different organic wastes. Dependency on process temperature", *Chemosphere,* Vol.62, No.9, 2006, pp. 1534–1542.

21. Raut, M. P., Prince William, S. P. M., Bhattacharyya, J. K., Chakrabarti, T., Devotta, S., "Microbial dynamics and enzyme activities during rapid composting of municipal solid waste—A compost maturity analysis perspective", *Biores. Technol.,* Vol.99, No.14, 2008, pp. 6512–6519.

22. Ros, M., García, C., Hernández, T., "A full scale study of treatment of pig slurry by composting: Kinetic changes in chemical and microbial Properties" *Waste Manage.,* Vol.26, No.10, 2006, pp. 1108–1118.

23. Sánchez-Monedero, M. A., Roig, A., Paredes, C., Bernal, M. P., "Nitrogen transformation during organic waste composting by the rutgers system and its effects on pH, EC and maturity of the composting mixtures", *Biores. Technol.,* Vol.78, No.3, 2001, pp. 301–308.

24. Shen, Y., Ren, L., Li, G., Chen, T., Guo, R., "Influence of aeration on CH_4, N_2O and NH_3 emissions during aerobic composting of a chicken manure and high C/N waste mixture". *Waste Manage.,* Vol.31, No.1, 2011, pp. 33–38.

25. Tiquia, S. M., "Evolution of extracellular enzyme activities during manure composting", *J. Appl. Microbiol.,* Vol.92, No.4, 2002, pp. 764–775.

26. Tiquia, S. M., Wan, J. H. C., Tam, N. F. Y., "Microbial population dynamics and enzyme activities during composting", *Compost Sci. Util.,* Vol.10, No. 2, 2002, pp. 150–161.

27. Wang, W., Wang, X., Liu, J., Ishii, M., Igarashi, Y., Cui, Z., "Effect of oxygen concentration on the composting process and maturity", *Compost Sci. and Util.,* Vol.15, No.2, 2007, pp. 184–190.

28. Xiao, Y., and Zeng, G.M., "Continuous thermophilic composting (CTC) for rapid biodegradation and maturation of organic municipal solid waste." *Biores. Technol.,* Vol.100, No.20, 2009, 4807–4813.

29. Zhang, W., Wu, S., Ji, H., KOLBE, H., "Estimation of agricultural non-point source pollution in China and the alleviating strategies I. Estimation of agricultural non-point source pollution in China in early 21 Century", *Scientia Agricultura Sinica,* Vol.37, No.7, 2004, pp. 1008–1017.

Trimethylamine Biofiltration and Isolation of a TriMethylamine-Degrading Strain from the Biofilter

JUN YIN[1,2,*] and WENFENG XU[3]

[1]School of Environmental Science & Engineering, Zhejiang Gongshang University, Hangzhou 310012, P.R. China
[2]Department of Environmental Engineering, Zhejiang University, Hangzhou 310029, P.R. China
[3]Hangzhou Academy of Environmental Science, Hangzhou 310014, P.R. China

ABSTRACT: A bacterium colonized in a laboratory-scale compost biofilter fed with trimethylamine (TMA) was isolated and characterized. The compost biofilter was operated with an influent TMA for 60 days. Results demonstrated that nearly all influent TMA may be removed in the biofilter. A microbial isolate TDB1 was selected based on its efficiency for maximum and faster biodegradation of TMA. It may grow both aerobically as well as anaerobically under nitrate reducing conditions with TMA as a sole carbon and energy source. According to 16S rDNA gene sequencing, strain TDB1 was assigned to the species Paracoccus aminovorans.

INTRODUCTION

TRIMETHYLAMINE (TMA) is potentially toxic and a likely carcinogenic volatile organic compound responsible for strong odor emissions. It is also a threat to public health because of its tissue-corrosive and tissue-penetrative properties. TMA is often released from the fish-meal manufacturing processes [1–3], the wastewater treatment process, waste disposal via a landfill, livestock farming, and hog manure [4–7]. TMA has also been known to inhibit synthesis of macromolecules such as DNA, RNA, and proteins as well as having a teratogenic effect on animal embryos [8]. Thus, microbial degradation would be useful to eliminate TMA from contaminated environments.

Biofiltration is believed to be one of the best technologies in terms of its technical and economical aspects and especially for treatment of low-concentration polluted air streams. Under proper conditions, high removal efficiencies may be achieved and the process is environment friendly [9,10]. Few reports have been made related to bioconversion of TMA as a sole target in biofilters. Chang *et al.* [7] used an aerobic biofiltration system containing entrapped mixed microbial cells (EMMC) for removal of $(CH_3)_3N$-dominant waste gases. Various natural or synthetic materials are widely used in biofiltration reactors. Most commonly, peat, bark, compost, and wood pellets are used. Synthetic media include ceramic, plastic, and glass. The choice of filter material is based on many parameters influencing attainable degradation performance but also on the avoidance of channelling and clogging problems. One kind of commercial compost was used which was mainly composed of pig manure and agricultural byproducts and was chosen to exploit microflora.

Recently, efforts are also being made to find high-performance biocatalysts. Inoculating bacteria in biofilters or simply favoring their growth seems to represent an interesting option for improving performance of biofilters treating air contaminated with volatile organic compounds. Conventional techniques of isolating bacteria were used to obtain pure bacterial stains. Until now, mainly two species of denitrifying bacteria, *Hyphomicrobium* sp. [11] and *Paracoccus* sp. [12, 13], have been reported as trimethylamine degraders. High elimination capacity of TMA was established in a biofilter filled with compost. The design was to isolate and identify TMA-degrading bacterial species from a compost biofilter using 16S rDNA gene sequencing. Results are useful for understanding mechanisms related to conversion of a target contaminant and for providing an economical and effective alternative for odor control.

MATERIALS AND METHODS

Biofiltration Experiment

The biofiltration experiment was performed using an

*Author to whom correspondence should be addressed.
E-mail: ceup_si@163.com

identical biofilter system (15 cm in diameter and 1.0 m in length) as described by Yin *et al.* [14] The bench-scale biofilter was divided into three equal sections for representative gas sampling from the bottom to the top along the column, Port 1, Port 2, and Port 3, respectively. Sections were flanged and each section could be dismantled to replace and sample filter material and to clean filter columns before and after use. TMA gas was made by injecting a TMA-containing solution into a mixing bottle using a syringe pump and a gas-tight syringe. Inlet air from the air pump was humidified to prevent the biofil biofilter matrix from drying and then it flowed into the biofilters mixed with TMA-containing gas. The gas inlet flow was controlled by a rotameter. TMA concentration by gas flow was kept constant by adjusting the injection rate of the solution and flow rate of the air stream. TMA concentration was initially set at 19.2 mg/m^3 and then was gradually increased from 19.2 to 57.2 mg/m^3 after 14 days. TMA was provided as sole carbon source and nitrogen source. Compost was used as packing material for the biofilter. Compost was a commercial product and was composed mainly of pig manure and agricultural by-products.

Bacterial Isolation

Compost samples were collected from the bottom layer of the biofilter. Compost (10 g) was placed directly into 90 mL of sterile mineral medium (i.e., 1.0 g of KH_2PO_4, 2.6 g of K_2HPO_4, 0.2 g of $MgSO_4·7H_2O$, 0.2 g of NH_4Cl 0.2 g, 0.25 g of KCl, 0.01% yeast extraction, 1,000 mL of distilled water, and a pH of 7.2) and was shaken for 15 min. A series of dilutions were made to reduce cells in samples. One mL of diluted sample was spread onto the surface of the mineral medium containing TMA in petri dishes and inoculated at 30°C and allowed to grow for 48–72 h. A single developed colony was picked on the TMA-mineral medium plates and subcultured to purification. Pure bacterial strains were obtained after successive transfer of individual colonies in TMA-mineral medium plates and incubated for 24 h at 30°C. After purity tests microorganisms were subjected to an extensive phenotypic investigation including cell morphology, Gram staining, and carbon and nitrogen source typing.

16S rDNA Sequencing and Data Analysis

DNA isolation and genomic DNA extraction from isolated cultures was performed as described by Ausubel *et al.* [15]. Universal bacterial 16S rDNA gene primers corresponding to the *Escherichia coli* position 8f and 1541r were used for polymerase chain reaction (PCR) amplification of the 16S rDNA gene. The forward primer 8f was 5′-AGAGT TTGAT CCTGG CTCAG-3′. The reverse primer sequence R1541 was 5′-AAGGA GGTGA TCCAG CCGCA-3′. These 50-μl reactions were performed using Taq polymerase with the following thermocycling program: $1 \times$ (2 min, 94°C), $30 \times$ (1 min, 94°C; 1 min, 56°C; and 2 min, 72°C), $1 \times$ (10 min, 72°C), and $1 \times$ (10 min, 60°C). All reactions were run using an Eppendorf Thermal Cycler (Hybaid, Teddington, Germany). PCR products were purified using a QIAquick PCR purification kit (Qiagen, Valencia, Calif.). Purified PCR products were sequenced by the Shenyou Biotechnology Company (Shanghai, China). Sequence was initially analyzed at the NCBI server (http://www.ncbi.nlm.nih.gov/) using the BLAST (blastn) tool. Corresponding sequences were downloaded.

Performance of the Strain under Aerobic and Anaerobic Conditions

All aerobic batch cultivations were carried out in 500-mL Erlenmeyer flasks containing 100 mL of medium. Flasks were shake-incubated at 30°C at 110 rpm. Strict anaerobic techniques were followed for anaerobic medium preparation, for aseptic handling, and for sampling of denitrifying cultures throughout the study. 100 mL of MSM with 30 mM nitrate was dispensed into a 125 mL serum bottle. Nitrogen gas was passed through an oxygen-trap filter (Chemical Research Supplies, Addison, IL) and was continuously flushed during dispensing of the medium. It was placed into the bottle for 5 min before it was tightly closed with a butyl-rubber stopper and aluminium seal. The redox potential of the medium was reduced by adding an anoxically prepared stock solution of Na_2S (0.2 M) to a final concentration of 0.2 mM. To avoid oxygen contamination during withdrawal of culture samples after sampling, nitrogen gas was additionally supplied. All cultures were incubated in the dark at 30°C and 110 rpm.

Analytical Methods

Cell growth was determined by the optical density (OD) of cultures at 650 nm using a spectrophotometer (Beckman, Fullerton, CA). During incubation, 2mL of culture fluid was sampled. Samples were filtered through a PVDF 0.22-μm-pore-size Millipore filter

and stored at –20°C until analyzed. Trimethylamine, dimethylamine, and methylamine were analysed in a gas chromatograph (GC) (SP-2000, Shandong, China) equipped with a glass column packed with GDX-401 coated with 4% PEG-20M + 1% KOH and with a flame-ionization detector. Injector temperature was 180°C, the detector temperature was 110°C, and the oven temperature was 180°C. Nitrogen at 40 mL/min was used as a carrier gas for GC analysis. Ammonia concentration was determined by the spectrophotometric method using Nessler reagent. Nitrite and nitrate were analysed using standard analytical methods (Chinese Standard Methods for the Examination of Water, 2002).

RESULTS AND DISCUSSION

TMA Removal

Compost had lower bulk density and porosity and therefore was easily compressed. Properties of lower bulk density and higher gas resistance for compost indicated that compost had a higher volumetric specific area for microbial growth. Bardke *et al.* [16] reported that media with a higher volumetric specific area were more efficient than those with a lower specific area for removing VOCs from gas streams. Therefore, the compost biofilter was expected to achieve better effectiveness in terms of TMA removal.

Results from removal of TMA by the biofilter is displayed in Figure 1. During the experiment, removal efficiency (*RE*) of TMA maintained 100% (i.e., no TMA detected). It was noticed that because the biofilter was operated in an upward-flow regime a majority of TMA

was removed in the first section (Section 1). From day 45 TMA in the effluent of Port 1 was detected (See Figure 1), whereas for the other ports no TMA was observed. No NH_3 was detected during the initial period at any port before day 15 indicating complete elimination of TMA through sorption and absorption. However, on day 28 a steadily increasing concentration of NH_3 was observed in Port 1 which indicated the absorbed TMA had been degraded into NH_3 by microorganisms in the packing material. Highest concentration of NH_3 was detected in the effluent of Port 1 but little was detected in Port 2 and 3 (data not shown). It may be estimated that biodegradation of TMA mostly occurred in the first section of the biofilter. Ammonia generated in Section 1 was absorbed and partially nitrified in the upper sections. Due to relatively low NH_3 loading nearly all NH_3 was eliminated from the gas. These results indicate that the biofilter may remove all potential odor and elimination ability was high.

Metabolic products including pH, ammonia, nitrite, and nitrate in compost were analysed within Section 1. Variations of pH, ammonia-N, nitrite-N, and nitrate-N contents in the biofilter are displayed in Figure 2. Discussed previously, TMA in the medium was biodegraded into NH_3. Content of NO_3^--N from day 26 remarkably increased indicating that nitrification had taken place. Ammonia was continuously transformed into NO_3^--N by nitrifiers which accumulated in each section and resulted in a pH decline. After day 39, the content of NO_4^+-N in section 1 suddenly dropped and was probably attributed to the decline of sorption of NH_3 with decreasing moisture from 67.2% to 59.2% (data not shown).
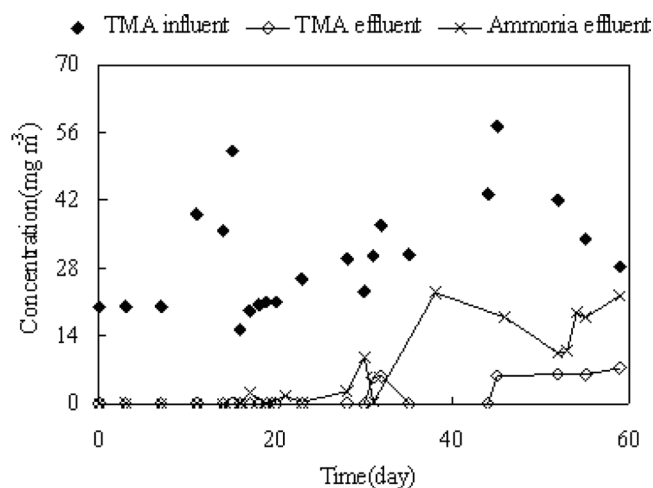

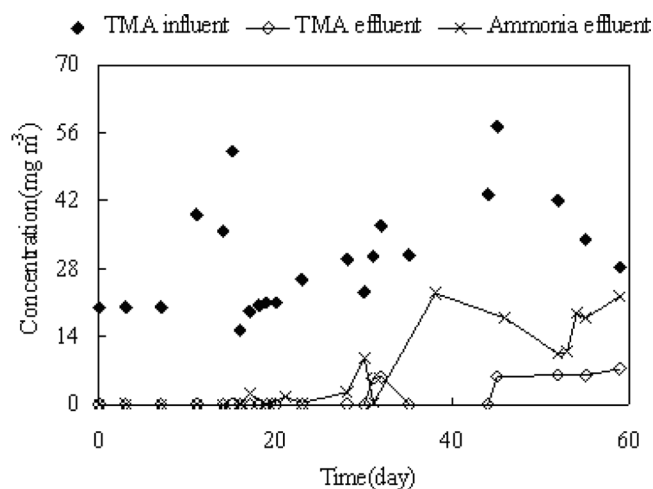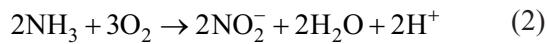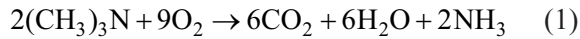**Figure 1.** *Removal of TMA in Section 1 of the biofilter.*

Figure 2. *Variations of pH, ammonia-N, nitrite-N, and nitrate-N contents at section 1 of the biofilter.*

Mechanism of Biodegradation of TMA

According to results, TMA elimination mechanisms by microbial communities in the packing material may properly be proposed with the following reaction equations Equation (1), Equation (2), and Equation (3):

$$2(CH_3)_3N + 9O_2 \rightarrow 6CO_2 + 6H_2O + 2NH_3 \quad (1)$$

$$2NH_3 + 3O_2 \rightarrow 2NO_2^- + 2H_2O + 2H^+ \quad (2)$$

$$2NO_2^- + O_2 \rightarrow 2NO_3^- \quad (3)$$

It was discovered that there was NH_3 in the effluent gas stream from Section 1 of the biofilter which indicated degradation of TMA carried out by TMA-degrading bacteria and hydrolysis of the influent TMA to NH_3 was evident [See Equation (1)]. NH_3 products could further be successfully converted to NO_2^--N [See Equation (2)] and then to NO_3^--N [See Equation (3)] and accumulated in the medium. Compost with features of higher volumetric specific area and better water-holding capacity could help maintain an advantageous medium for growth and activity of ammonia-oxidizing bacteria. Also, Bardtke [16] results were confirmed. It needn't be inoculated with nitrifying bacteria because ammonia-oxidizing bacteria had already existed there [14].

Isolation of Bacterium

Since accurate identification of environmental bacteria is essential in order to achieve a better understanding of the biodegradation process, microbial isolation and identification were performed and evaluated. Using agar plates containing TMA as a sole carbon source colonies are pinhead size, circular, smooth, convex, entire, transparent, and yellowish white after 10 days of incubation. The isolate, strain TDB1, is gram-negative, non-motile, non-spore forming, and a short rod (0.5×0.9–1.2 μm). Figure 3 displays gram-staining identifications from the compost biofilter. The culture exhibited good degradation ability in a pH range from 6.5 to 8.0 and in a temperature range from 30 to 37°C. No addition of vitamins is required. Electron acceptors are oxygen and nitrate. Physiological reaction profile of strain TDB1 was characterized by successful growth on the TMA, DMA, and MA. This property was also found for *Paracoccus aminovorans*. Glucose, mannitol, acetate, and formate may serve as carbon sources. However, glutamate and malate cannot be used. Amino acid, sodium nitrite, ammonium sulphate, and urea may serve as nitrogen sources. Nitrate may not be utilised as a nitrogen source. Yet in contrast, *Paracoccus aminovorans* could not utilize formate. Strain TDB1 could use urea as nitrogen source and converted nitrate to nitrite under anaerobic conditions.

Bacterial Identification Based on 16S rDNA

Using internal primers the 509 bp sequence of amplified 16S rDNA gene fragment was determined. Sequence analysis results for 16S rDNA are displayed in Figure 3. The BLASTN search indicated that the organism belongs to *Proteobacteria,* α subdivision, *Paracoccus* genus. According to the BLASTN analysis, the 16S rDNA nucleotide sequence from the TMA-degrading bacterium was 98.8% identical to a corresponding sequence from *Paracoccus aminovorans*
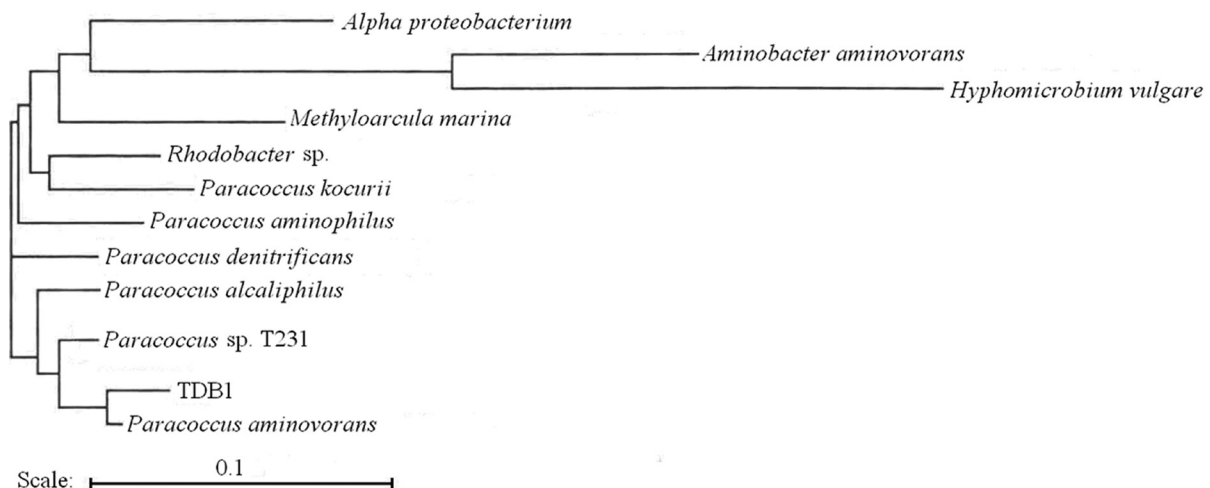

Figure 3. *Phylogenic tree of strain TDB1 based on 16S rDNA sequence analysis.*

(GenBank accession number D32240). Kim *et al.* [17] first reported that a strain T231 had two different pathways for aerobic and anaerobic degradation of trimethylamine. Based on 16S rDNA analysis the strain was identified as a Paracoccus sp.

Aerobic Degradation of TMA

Under oxic conditions biodegradation of TMA as a sole carbon and energy source by strain TDB1 is displayed in Figure 4. Cell growth entered into the exponential-growth phase after 10 hours. Within 24 hours the biomass reached a maximum value followed by a decline in biomass concentration. Aerobic degradation of TMA supported cell growth indicates the strain utilized these substrates as a carbon source as well as an energy source. Strain TDB1 completely degraded 8.9 mM TMA in 15 h (See Figure 4). During degradation of TMA dimethylamine (DMA) was accumulated and subsequently degraded suggesting DMA is a metabolic intermediate of TMA. Ammonium concentration followed a similar pattern to biomass growth. It concomitantly increased during degradation of TMA and then experienced an obvious decline. It has been demonstrated that ammonium is an end metabolic product of degradation of methylated amines. The fact that ammonium was released in the culture fluid in each case suggests methylated amines were completely metabolized by this strain.

Anaerobic Degradation of TMA

Under denitrifying conditions with 30 mM nitrate, the anaerobic biodegradation of TMA by strain TDB1 is displayed in Figure 5. Cell growth entered into the exponential-growth phase after 12 hours. In the presence of 30 mM nitrate strain TDB1 completely degraded 16 mM trimethylamine in 42 h [See Figure 5(a)]. During anaerobic degradation dimethylamine and methylamine were produced and accumulated. When TMA was degraded completely at 42 h the DMA concentration reached a maximum at 15 mM and subsequently degraded. At 60 h MA accumulated to 1.9 mM. This suggests TMA was metabolized via DMA and MA. During degradation of TMA concomitant nitrate consumption and cell growth were observed [See Figure 5(b)]. Nitrite, an intermediate of nitrate reduction, was detected during this culture period but its concentration was very low suggesting nitrate was an electronic acceptor during degradation of TMA.

(a)

(b)

Figure 5. *Anaerobic degradation of TMA by strain TDB1 in the presence of 30 mM nitrate.*

Figure 4. *Aerobic degradation of TMA by strain TDB1.*

Enzymes related to TMA degradation were not assayed. According to the literatures some enzymes have been reported to catalyze methylamine metabolism such as methylamine oxidase [17], methylamine dehydrogenase [18], *N*-methylglutamate synthase [19], and *N*-methylalanine dehydrogease [20]. Cell-free extracts of *Paracoccus* sp. T231 grown on trimethylamine u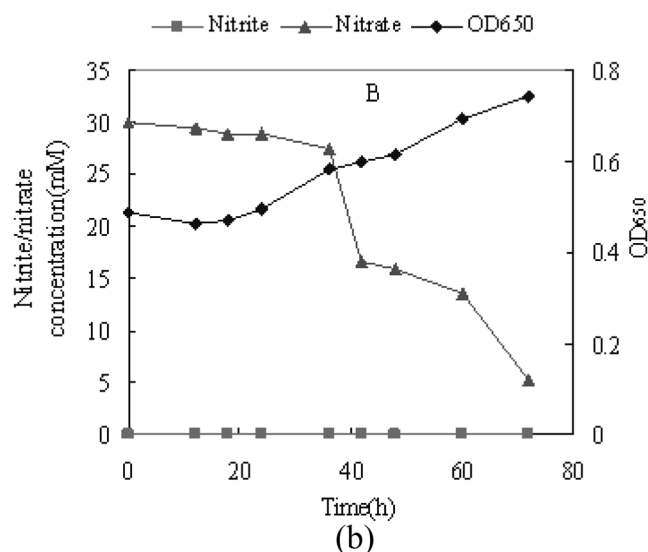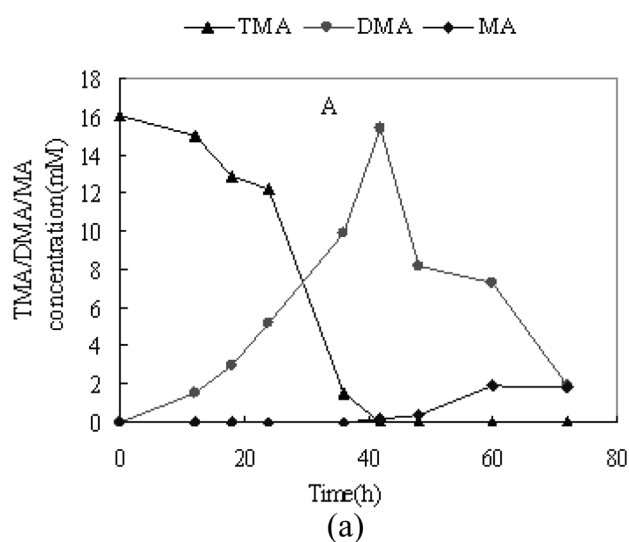nder aerobic conditions created (i.e., detected) the following enzyme activities: trimethylamine mono-oxygenase, dimethylamine mono-oxygenase, methylamine mono-oxygenase, and trimethylamine *N*-oxide demethylase [3]. Trimethylamine dehydrogenase and dimethylamine dehydrogenase were found in cells grown under denitrifying conditions which suggests the pathway for anaerobic degradation of trimethylamine is different from the pathway for aerobic degradation. *Hyphomicrobium* X oxidized trimethylamine with trimethylamine dehydrogenase both aerobically and under anaerobic denitrifying conditions.

CONCLUSIONS

A laboratory-scale biofilter was operated with an influent TMA concentration of 19.2–57.2 mg/m^3 for 60 days. TMA was successfully removed by the biofilter with an efficiency of 100% and most of which was eliminated in the first section. Evaluating analysis of variations for the properties of the compost packing material it was observed that compost not only treats TMA effectively but also eliminates NH_3 produced completely by the nitrification process. According to above phenomenon, TMA elimination mechanisms by microbial communities in the packing material may properly be proposed. First, TMA was biodegraded to NH_3. NH_3 produced may further be converted to NO_2^--N and then to NO_3^--N accumulating in the compost.

A bacterium (TDB1) colonized in the compost biofilter was isolated and characterized which is identified as *Paracoccus* sp. by biochemical methods and 16SrRNA analysis. The strain may grow both aerobically as well as anaerobically under nitrate reducing conditions with TMA providing a sole carbon and energy source. It aerobically degraded trimethylamine via dimethylamine and methylamine and released the ammonium ion into the culture fluid as a metabolic product. The strain also degraded trimethylamine under denitrifying conditions and consumed nitrate. This demonstrates that complete degradation of trimethylamine was coupled with nitrate reduction. According to the 16S rDNA gene sequencing the isolated strain was assigned to the species *Paracoccus aminovorans*.

REFERENCES

1. Sandberg, M. and B. K. Ahring, "Anaerobic treatment of fish meal process waste-water in a UASB reactor at high pH", *Appl. Microbiol. Biotechnol.,* Vol. 36, No. 6, 1992, pp. 800–804.

2. Hwang, Y., T. Matsuo, K. Hanaki and N. Suzuki, "Removal of odorous compounds in wastewater by using activated carbon, ozonation and aerated biofilter", *Water Res.,* Vol. 28, No. 11, 1994, pp. 2309–2319.

3. Kim, S. G., H. S. Bae and S. T. Lee, "A novel denitrifying bacterial isolate that degrades trimethylamine both aerobically and anaerobically via two different pathways", *Arch. Microbiol.,* Vol. 176, No. 4, 2001, pp. 271–277.

4. Shieh, W. K. and D. J. Keenan, "Fluidized bed biofilm reactor for wastewater treatment", *Adv. Biochem. Eng.,* Vol. 33, 1986, pp. 131–169.

5. Leson, G. and A. M. Winer, "Biofiltration-an innovative air pollution control technology for VOC emission", *J. Air Waste Manage. Assoc.,* Vol. 41, No. 8, 1991, pp. 1045–1054.

6. Cao, N. J. and J. X. Du, "Production of fumaric acid by immobilized Rhizopus using rotary biofilm contactor", *Appl. Biochem. Biotechnol.,* Vol. 63-65, No. 1, 1997, pp. 387–394.

7. Chang, C. T., B. Y. Chen, I. S. Shiu and F. T. Jeng, "Biofiltration of trimethylamine-containing waste gas by entrapped mixed microbial cells", *Chemosphere,* Vol. 55, No. 5, 2004, pp. 751–756.

8. Guest, I. and D. R. Varma, "Teratogenic and macromolecular synthesis inhibitory effects of trimethylamine on mouse embryos in culture", *J. Toxicol. Environ. Health.,* Vol. 36, No. 1, 1992, pp. 27–41.

9. Kennes, C. and F. Thalasso, "Waste Gas Biotreatment Technology", *J. Chem. Technol. Biotechnol.,* Vol. 72, No. 4, 1998, pp. 303–319.

10. Burgess, J. E., S. A. Parsons and R. M. Stuetz, "Developments in odour control and waste gas treatment Biotechnology: a review", *Biotechnol. Advan.,* Vol. 19, No. 1, 2001, pp. 35–63.

11. Meiberg, J. B. M. and W. Harder, "Aerobic and anaerobic metabolism of trimethylamine, dimethylamine and methylamine in Hyphomicrobium X", *J. Gen. Microbiol.,* Vol. 106, No. 2, 1978, pp. 265–276.

12. Lipski, A., K. Reichert, B. Reuter, C. Spröer and K. Altendorf, "Identification of bacterial isolates from biofilters as *Paracoccus alkenifer* sp. nov. and *Paracoccus solventivorans* with emended description of *Paracoccus solventivorans*", *Int. J. Syst. Bacteriol.,* Vol. 48, No. 2, 1998, pp. 529–536.

13. Ohara, M., Y. Katayama, M. Tsuzaki, S. Nakamoto and H. Kuraishi, "Paracoccus kocurii sp. nov. a Tetramethylammonium-Assimilating Bacterium", *Int. J. Syst. Bacteriol.,* Vol. 40, No. 3, 1990, pp. 292–296.

14. Yin, J. and W. F. Xu, "Ammonia biofiltration and community analysis of ammonia-oxidizing bacteria in biofilters", *Biores. Technol.,* Vol. 100, No. 17, 2009, pp. 3869–3876.

15. Ausubel, F. M., R. Brent, R. E. Kingston, D. D. Moore, J. A. Seidman and J. G. Smith. 1997. *Current protocols in molecular biology,* New York: John Wiley and Sons.

16. Bardtke, D., K. Fisher and F. Sabo, "Air purification with biofilters, field of application and design criteria", in *Proceeding of the 80th Annual Meeting & Exhibition of Air & Waste Management Association;* pp. 87–106, 1987.

17. van Vliet-Smits, M., W. Harder and J. P. van Dijken, "Some properties of the amine oxidase of the facultative methylotroph *Arthrobacter* P1", *FEMS Microbiol. Lett.,* Vol. 11, No. 1, 1981, pp. 31–35.

18. Eady, R. R. and P. J. Large, "Microbial oxidation of amines. Spectral and kinetic properties of the primary amine dehydrogenase of *Pseudomonas* AM1.", *Biochem J.,* Vol. 123, No. 5, 1971, pp. 757–771.

19. Pollock, R.J. and L.B. Hersh, "*N*-methylglutamate synthetase. Purification and properties of the enzyme", *J. Biol. Chem.,* Vol. 246, No. 15, 1971, pp. 4737–4743.

20. Lin, M. C. M. and C. Wagner, "Purification and characterization of *N*-methylalanine dehydrogenase", *J. Biol. Chem.,* Vol. 250, No. 10, 1975, pp. 3746–3751.

Adsorption Behavior and Removal of Organic Materials from TNT Red Water by Lignite Activated Carbon

YIHE ZHANG[1,*], FANGFANG WEI[1], JING XING[1], FENGZHU LV[1], XIANGHAI MENG[1] and PAUL K. CHU[2]

[1]*National Laboratory of Mineral Materials, School of Materials Sciences and Technology, China University of Geosciences, Beijing, 100083, China*

[2]*Department of Physics & Materials Science, City University of Hong Kong, Tat Chee Avenue, Kowloon, Hong Kong, China*

ABSTRACT: Red water produced by manufacturing of 2,4,6-trinitrotoluene (TNT) is treated by lignite activated carbon (LAC) which is much cheaper than common activated carbon. Optimized conditions for adsorption were determined and experimental results suggested pH, initial concentration, time, and adsorbent dose effect adsorption. The adsorption process follows a pseudo-second-order kinetics model controlled by pore diffusion and an adsorption isotherm may be fitted using the Langmuir model. Most organic components in red water are adsorbed by hydrogen bonds between the LAC and organic materials. Results suggest LAC is an alternative for treatment of red water.

INTRODUCTION

ACCORDING to pollutant characteristics, TNT waste water may be categorized as yellow water, red water, pink water, and condensates [1]. TNT red water is an aqueous effluent produced during the purification step of trinitrotoluene (TNT) production. During the purification stage, sodium sulfite is added to react with the asymmetrical nitrotoluenes leading to formation of dinitrotoluene (DNT) sulfonates (2,4-DNT-3-sulfonate and 2,4-DNT-5-sulfonate) [2]. Red water contains products of incomplete nitrate compounds as well as other complex by-products formed during nitration and purification stages in addition to DNT sulfonated compounds. They create concern related to environmental pollution and public health since most of them are toxic and mutagenic to humans and other animals even at low concentrations [3–6]. Dark red and opaque waste water has high concentrations of dissolved organics and tends to be difficult to handle.

Common treatment methods for TNT waste water include activated carbon adsorption [7–8], incineration, biodegradation [9], advanced oxidations such as oxidation with hydrogen peroxide/ozone [10], supercritical water oxidation [11], Fenton reagent oxidation, photocatalytic oxidation [12,13], and so on. Although incineration of TNT is one of the most effective and commonly used processes it is expensive due to high fuel costs [14]. Also, burning emits gaseous pollutants into the environment [15,16]. There have been relatively few studies on biodegradation of TNT in an aqueous medium and most previous studies on TNT biodegradation focused on treatment of TNT contaminated soils [17–19]. There are several challenges such as resistance under aerobic conditions in the presence of electron-withdrawing nitro constituents in explosives that inhibit electrophilic attack through enzymes [20]. Furthermore, biological methods require a longer degradation time. Since the method of advanced oxidations must be carried out under extreme reaction conditions it is difficult for many TNT plants to perform the costly task.

Activated carbon is frequently utilized to clean polluted water and it is feasible to use granular activated carbon (GAC) to treat drinking water contaminated with TNT. Maloney *et al.* [21] have evaluated an anaerobic fluidized bed reactor (FBR) composed of GAC in the treatment of TNT pink water. It can remove 99% of DNT and is a highly efficient method. Rajagopal and Kapoor [7] have studied adsorption characteristics of nitro-organics such as trinitrotoluene (TNT), dinitrotoluene (DNT), and nitrobenzene (NB) on GAC and obtained optimal conditions. A model has been developed to predict adsorption dynamics and the effects of various parameters on adsorption characteristics. Marinovic *et al.* [22] have investigated effects of dynamic TNT adsorption on GAC. Effects of temperature, concentration, and flow rate using a chromatographic system were examined and the possibility of desorb-

*Author to whom correspondence should be addressed.
E-mail: zyh@cugb.edu.cn

ing TNT from saturated activated carbon was explored. Vasilyeva *et al.* [23] have studied the oxidation mechanism of carbon on TNT and found that activated carbon can accelerate TNT oxidation forming unextractable residues. Strong binding may be attributed to catalyzed oxidation of the TNT methyl group, probably via a free radical mechanism involving chemisorption of the oligomers and polymerized products that do not desorb from micropores. Therefore, TNT oxidation and residue formation after adsorption by activated carbon increase effectiveness of activated carbon to decontaminate water.

It is important to find an economical and efficient method to remove TNT in spite of scattered success. LAC which is much cheaper than common activated carbon and seldom used to treat TNT red water was employed. The optimal conditions, thermodynamics, and kinetics of the adsorption process were also studied.

METHODLOGY

Materials

TNT red water was supplied by Dongfang Chemical Corporation, Hubei Province, China. LAC was supplied by Datang Co. Ltd. All other chemicals were analytical reagent grade.

Experimental Procedures

Batch experiments were carried out in a series of 100 mL conical flasks in which a certain quantity of LAC and 50 mL of TNT red water were added. Bottles were shaken in an SHA-BA water bath with a constant temperature oscillator at a speed of 150 rpm and temperature of $25 \pm 0.2°C$. Effects of pH and reaction temperature on TNT adsorption were investigated under specific conditions. Suspension was filtered rapidly with filter paper and the filtrate was used immediately to determine adsorption efficiency of LAC.

Analyses

TNT concentrations in the solutions were determined by sodium sulfite spectrophotometry using a 722 SP visible spectrophotometer (Shanghai Lengguang Instrument Co., Ltd) at 420 nm (Chinese Standardization, 1993). Organic compositions of TNT red water were determined by gas chromatography/mass spectrometry (GC/MS, GC6890/MSD5973 N, Agilent Corporation, USA). A sample of 1.0 μL was injected into the GC/MS operated from 40 to 280°C at a programmable rate of $2.0°C \ min^{-1}$. A DB-35 MS capillary column with an inner diameter of 0.25 mm and length of 60 m was adopted in the separation system. Helium gas was used as the carrier gas and introduced at a flow rate of $1.0 \ mL \ min^{-1}$. Dried red water samples were characterized by Fourier transform infrared spectroscopy (FTIR, Spectrum 100, Perkin Elmer). Adsorbent surface was examined using scanning electron microscopy (SEM, HITACHI S450) before and after adsorption experiments. Oxygen demand was determined using a COD rapid detector (5B-6, Lian-Hua Tech. Co., China).

RESULTS AND DISCUSSION

Water Quality Analysis

TNT red water is reddish brown and opaque containing high concentrations of TNT and chemical oxygen demand (COD). Waste water used in the experiments was diluted 100 times and important properties may be seen in Table 1. FTIR and GC/MS are used to identify composition of TNT red water and results are displayed in Figure 1 and Table 2. The infrared spectrum seen in Figure 1 displays characteristic bands of nitryl at 1539 and 1365 cm^{-1} and a characteristic band of heterocyclic nitrogen compounds at 616 cm^{-1}. GC/MS results seen in Table 2 indicate organic components in the TNT red water are complex and 3-methyl-6-nitrobenzoic acid, 2-methyl-3,5-dinitro-phenol, 1,3,5-trinitrobenzene, and 2,4,6-trinitrobenzene are the largest components appearing at 60 and 67 min.

Properties of LAC

Important properties of LAC which effect adsorption characteristics are provided in Table 3. LAC has high microporosity, iodine number, and BET surface area. However, the bulk density value is not very large

Table 1. Properties of Red Water Diluted 100 Times.

Sample	pH	COD (mg/L)	Solid Content (mg/L)	TNT (mg/L)	Turbidity	Chromaticity
Red water	6.20	1100 ± 20	1980	50.7	59.8	reddish brown 1×10³ times

Figure 1. *FTIR spectrum of red water.*

Table 3. Important Properties of LAC.

Properties	LAC
Specific surface area (m^2/g)	860.6
Average pore diameter (nm)	2.573
Porosity (%)	48.6
Total pore volume (ml/g)	0.785
Microporosity (%)	50.9
Iodine number (mg/g)	818.3
Bulk density (g/cm^3)	0.68
pH	6.7

Adsorption of Organic Materials from TNT Red Water

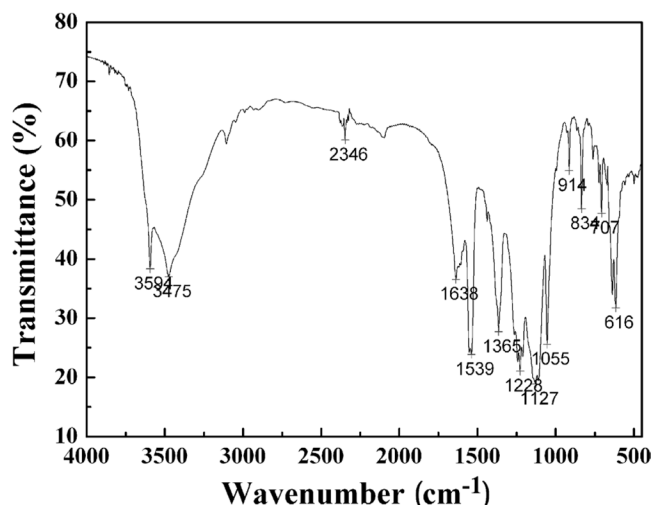### Effects of Adsorbent Aose

and from the pH values it may be concluded that the LAC has acidic characteristics. Types and amounts of surface functional groups in the LAC samples are determined using Boehm analysis and results are provided in Table 4. Amounts of carboxylic, lactonic, and phenolic groups are determined by neutralizing them with basic solutions of different base strengths such as $NaHCO_3$, Na_2CO_3, NaOH, and C_2H_5ONa. Basic group content was determined by titration using HCl.

As seen in Table 4, LAC contains mainly oxygen groups with weakly acidic properties and basic groups. Boehm analysis suggests that the amount of carboxylic functional groups is much larger than that of the basic groups. It is believed that acidic functional groups cause adsorption of organic compounds because removal of organic compounds is positively affected by acidic functional groups having hydrogen bonds.

Adsorbent dose is an important parameter because it determines the capacity of the adsorbent for a given initial concentration of adsorbate. Effects of the adsorbent dose on TNT degradation are illustrated in Figure 2. Removal rates of TNT increase from 18.0 to 84.7% and those of COD increase from 15.7 to 70.3% as quantities of LAC are increased from 0.05 to 2.0 g. When quantity reaches 5.0 g, removal rates of TNT and COD are 95.8 and 87.6%, respectively. Results indicate that TNT and COD removal efficiency is enhanced by larger adsorbent dose. This is because total specific surface area and active sites on the LAC increase. When adsorbent dose increases degradation of TNT and COD is favored. However, rates are not affected significantly when dose is increased from 2.0 to 5.0 g and accordingly, an LAC dose of 2.0 g/50 ml is considered an optimal dose for TNT removal in our experiments.

Table 2. GC/MS Results of TNT Red Water.

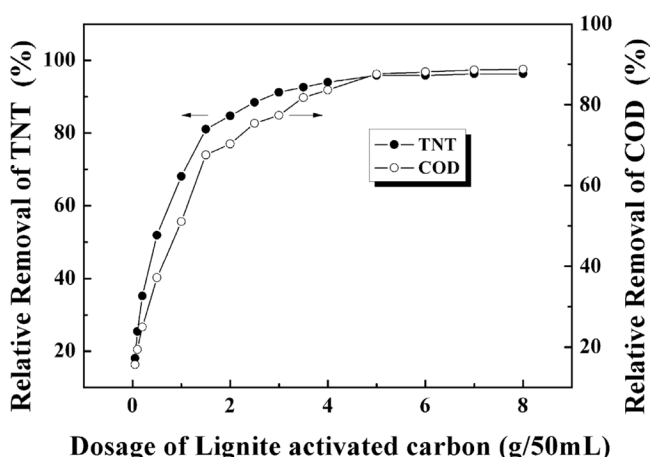| Retention Time (min)	Assignments
30.0	2-Nitrotoluene
33.8	4-Nitrotoluene
34.6	3-Methyl-2-nitrophenol
36.7	5-Methyl-2-nitrophenol
50.8	2,6-Dinitrotoluene
53.5	2,4-dinitrotoluene
55.0	2,5-Dinitrotoluene
60.1	3-Methyl-6-nitrobenzoic acid
60.6	2-Methyl-3,5-dinitrophenol
67.1	1,3,5-Trinitrobenzene
67.8	2,4,6-Trinitrotoluene
79.7	3,5-Dinitro-*p*-toluidine

Figure 2. *Effects of adsorbent doses on adsorption.*

Table 4. Boehm Analysis Results of LAC.

Material	Basic Groups	Carboxylic Groups	Lactonic Groups	Phenolic Groups	Total Acidic Groups
LAC	0.23	1.30	0.14	.031	1.75

Effects of Exposure Time

In order to determine optimal adsorption time for activated carbon used in this study, effects of exposure time are determined at 298 K. Seen in Figure 3, removal rates of TNT and COD increase gradually with time. Initially, TNT adsorption rate is high but diminishes gradually with time. It may be because adsorption area decreases as the surface of LAC is covered by TNT and other organic compounds from red water. Minimum contact time required to reach equilibrium is 6 hours for LAC and in our experiments soaking time was fixed at these values to make sure equilibrium is achieved.

To analyze adsorption rates and kinetics of organic materials adsorption from TNT red water by the LAC, three kinetic models, namely pseudo-first-order, pseudo-second-order, and intra-particle diffusion models were evaluated. The Lagergren's equation is one of the most widely used rate equations to describe adsorption from a liquid phase [24]. The linear form of the pseudo-first-order rate expression of Lagergren's equation [Equation (1)] is given as:

$$\log(q_e - q_t) = \log q_e - \frac{k_f}{2.303}t \qquad (1)$$

where, q_e and q_t are amounts of the TNT adsorbed (mg/g) at equilibrium and at time t (min) and k_f is the rate constant. Values of k_f and q_e for adsorption by LAC are determined from the plot of $\log(q_e - q_t)$ versus t [See Figure 4(a)].
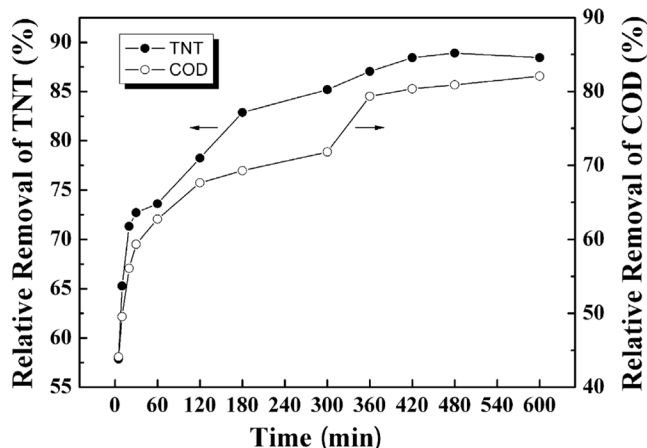

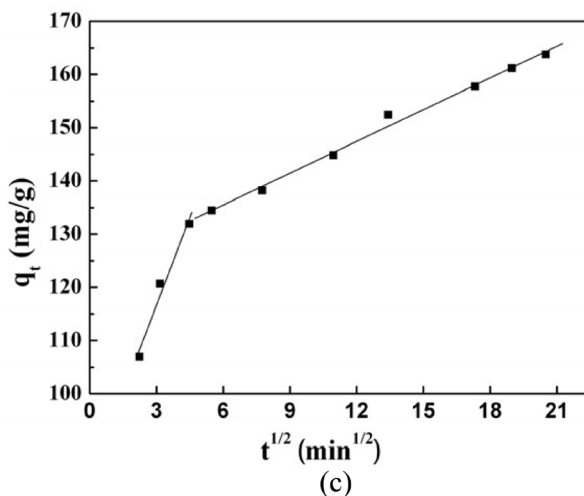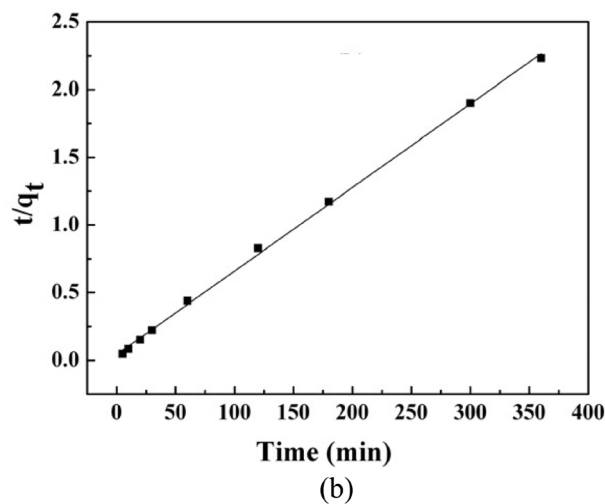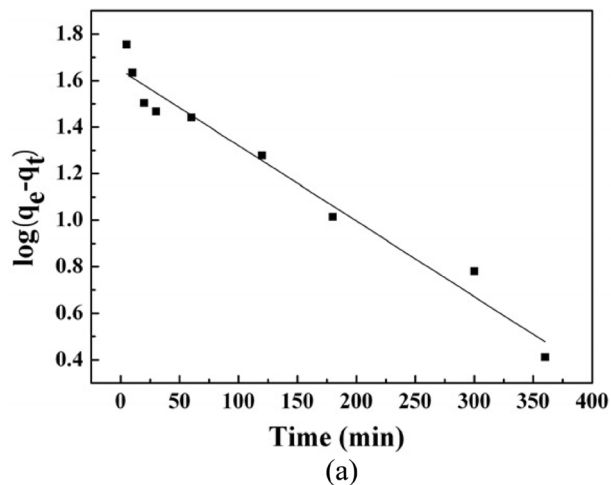**Figure 3.** Effects of exposure times on adsorption.

Figure 4. (a) Pseudo-first-order model, (b) Pseudo-second-order model, and (c) Intra-particle diffusion model pertaining to TNT removal from red water by LAC.

Adsorption kinetics may be described by the following pseudo-second-order process [Equation (2)] [25]:

$$\frac{t}{q_t} = \frac{1}{k_s q_e^2} + \frac{1}{q_e} t \qquad (2)$$

where, q_e and q_t have the same connotation as mentioned previously and k_s is the rate constant in the pseudo-second-order kinetics model. The plot of t/q_t versus t is displayed in Figure 4(b). Values of k_s and q_e may be calculated from the slope and intercept of the plot in Figure 4(b).

Concentration dependence of the adsorption rate is frequently used to analyze the nature of the rate-determining step. Use of the intra-particle diffusion model has been explored in this regard and is represented by Equation (3) [14]:

$$q_t = k_{ip} t^{1/2} + C \qquad (3)$$

where k_{ip} is the intraparticle diffusion rate constant and C is the intercept related to the thickness of the boundary layer. The plot of q_t versus $t^{1/2}$ is seen in Figure 4(c).

Constants for kinetic models are provided in Table 5. It may be concluded that adsorption of TNT by LAC does not follow a pseudo-first-order model since calculated adsorption capacity was 44.19 mg/g and very different from an experimental adsorption capacity of 163.79 mg/g. A better correlation coefficient (0.999) in contrast and smaller difference between the calculated saturated adsorption capacity and experimental adsorption capacity are observed using the pseudo-second-order model. Using the intra-particle diffusion model, the fitted curve is divided into two regions, surface diffusion and internal diffusion, due to influence by boundary layer diffusion and internal diffusion, respectively. The rate parameter k_{ip1} (11.01) calculated from the first region is higher compared to k_{ip2} (1.99) from the second stage indicating surface diffusion is much faster than internal diffusion.

Adsorption Isotherms
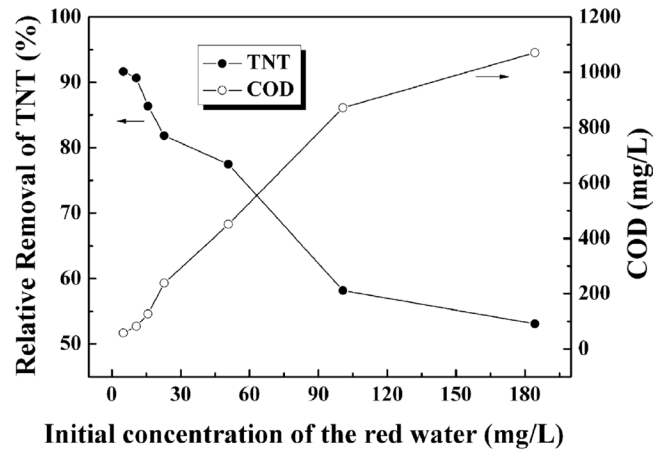
Figure 5 displays results obtained from a series of

Figure 5. *Effects of initial concentrations on adsorption.*

experiments performed using different concentrations of waste water. Removal rates of TNT decrease approximately from 92 to 53% and COD values increase from 51 to 95 mg/l when initial concentrations are changed from 10 to 200 mg/l (See Figure 5). Although higher concentrations of TNT red water can promote adsorption, the number of active sites on the LAC is limited. Superfluous adsorbates cannot be adsorbed when a balance is reached. Hence, the adsorption rate is reduced and results suggest waste water should be diluted before treatment to improve adsorption efficiency.

The equilibrium relationship between adsorbent and adsorbate is described by the adsorption isotherms. Two adsorption isotherm Equations (4) and (5) are used in the present study, namely Langmuir [23] and Freundlich [26]. Applicability of isotherm models was compared by evaluating correlation coefficients. Linear forms of the Langmuir and Freundlich isotherms are represented by the following equations [Equations (4) and (5)]:

$$\frac{C_e}{q_e} = \frac{C_e}{q_m} + \frac{1}{q_m b} \qquad (4)$$

where q_e is the amount (mg/g) adsorbed at equilibrium concentration C_e (mg/L), and q_m (mg/g) and b (L/mg) are the maximum adsorption capacity of the adsorbent and adsorption energy coefficient, respectively.

Table 5. Pseudo Rirst-order, Pseudo Second-order, and Intraparticle Diffusion Kinetic Parameters for TNT in Red Water by LAC.

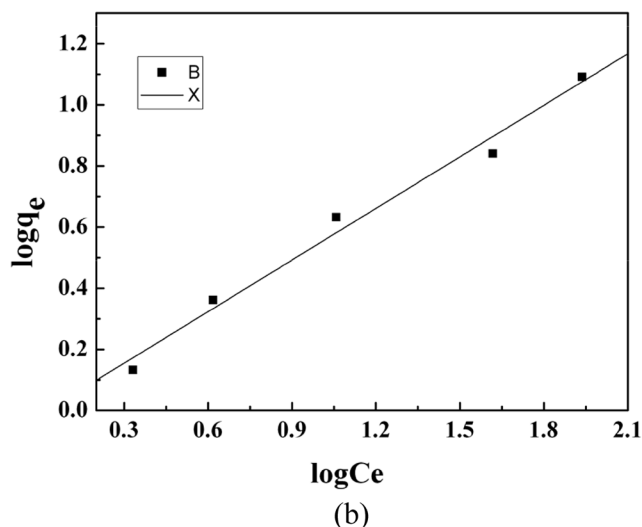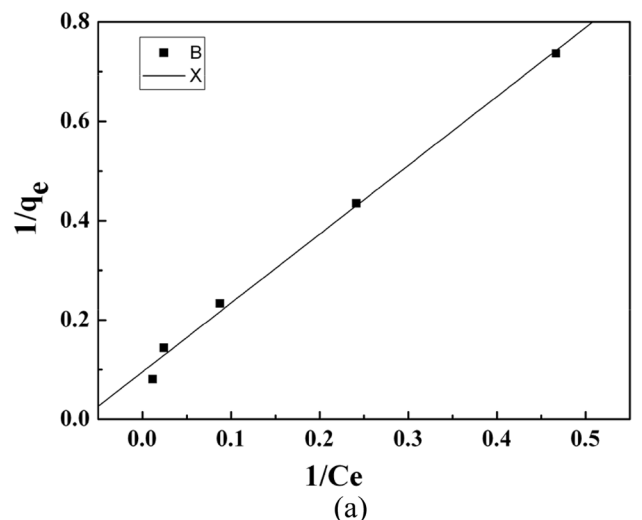| Pseudo First-order				Pseudo Second-order				Intraparticle Diffusion			
$k_f \times 10^{-3}$ (min^{-1})	q_e(exp) (mg/g)	q_e(cal) (mg/g)	R^2	$k_s \times 10^{-4}$ (min^{-1})	q_e(exp) (mg/g)	q_e(cal) (mg/g)	R^2	k_{ip1} (mg/g min)	R^2	k_{ip2} (mg/g min)	R^2
7.37	163.79	44.19	0.9689	9.11	163.79	161.29	0.9990	11.01	0.9503	1.99	0.9908

(a)

(b)

Figure 6. *Adsorption isotherms for the (a) Langmuir and (b) Freundlich models.*

$$\log q_e = \log K_F + \frac{1}{n} \log C_e \qquad (5)$$

where K_F is Freundlich constant (mg/g) associated with the adsorption capacity and $1/n$ is the heterogeneity factor related to the adsorption intensity or surface heterogeneity.

Figure 6 displays adsorption isotherms according to the Langmuir and Freundlich models. Theoretical pa-
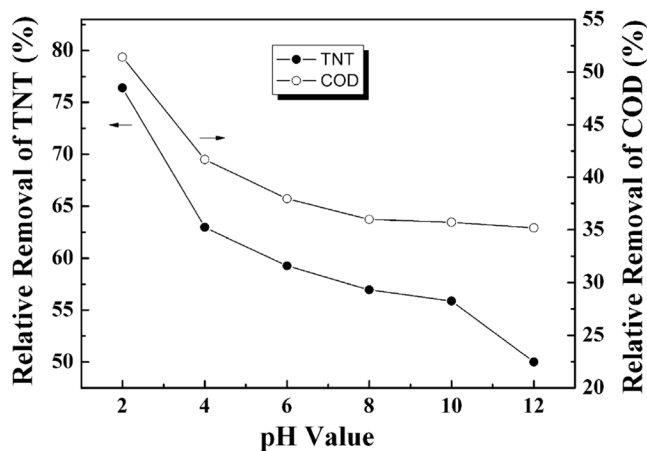

Figure 7. *Effects of pH values on adsorption.*

rameters of adsorption isotherms along with regression coefficients are provided in Table 6. The Langmuir isotherm model has the highest values of regression coefficients compared to other isotherm models suggeting the homogeneous nature of the adsorbent. Maximum adsorption capacity and Langmuir constant are calculated from slope and intercept of linear plots C_e/q_e versus C_e which gives a straight line of slope $1/q_m$ corresponding to complete monolayer coverage (mg g^{-1}) and an intercept of $1/q_m b$.

The effects of pH on solid/liquid adsorption processes are significant in such reactions. Here, adsorption of TNT by LAC over a broad pH range (2–12) is performed in red water that has been diluted 100 times at a temperature of 298 K and at an agitation speed of 150 rpm. Results are provided in Figure 7. The pH indeed has a large impact on adsorption characteristics. Adsorption efficiency and removal rate of COD decreases with increasing pH. The optimal pH for TNT removal is 2 and adsorption is not easy when the pH is higher than 10. There are large amounts of aromatic compounds with nitro groups and both oxygen and nitrogen are electronegative elements with oxygen having a higher electronegativity [27]. The nitro groups may be bonded easily to hydrogen thereby accelerating extraction of TNT. When pH is higher than 10, there is not enough hydrogen and adsorption is hindered. A pH of 2.0 is optimal and is now used in subsequent experiments.

Table 6. *Langmuir and Freundlich Isotherm Model Constants and Correlation Coefficients for Adsorption of TNT in Red Water on LAC.*

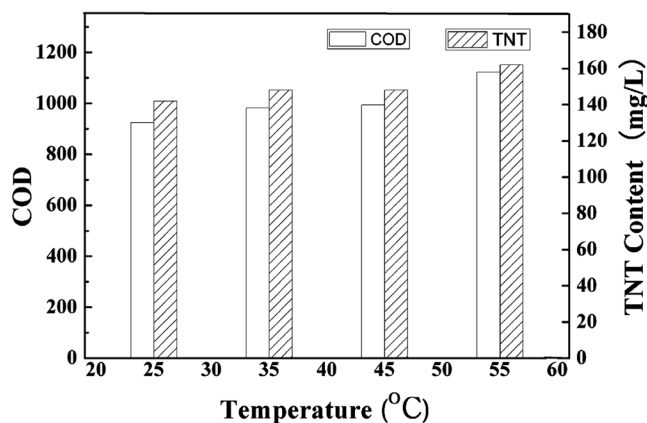| Temperature	Langmuir Constants			Freundlich Constants		
	q_m (mg/g)	b (L/mg)	R^2	K_f (mg/g(L/mg)$^{1/n}$)	$1/n$	R^2
25°C	160.45	0.069	0.9929	0.97	0.56	0.9808

Figure 8. *Effects of temperature on adsorption.*

Effects of Temperature

In order to better understand temperature effects on adsorption of TNT and removal rate of COD, experiments were conducted at 25, 35, 45, and 55°C and results are displayed in Figure 8. After adsorption, COD and TNT contents increase with temperature denoting that some kind of endothermic chemical interactions may have taken place during adsorption. In addition, increase in adsorption with temperature may enlarge pore size which may also affect carbon adsorption capacity [28]. However, increase in the COD and TNT contents is not obvious. This may be because a higher temperature favors agglomeration up to a certain temperature limit beyond which desorption becomes more important. Hence, adsorption rate is reduced with time

[29]. Results reveal that temperature effects on adsorption are not significant on account of the small energy of liquid adsorption. Consequently, room temperature is the desirable temperature in practice.

Morphology of Adsorbent

SEM micrographs of activated carbon are displayed in Figure 9. SEM images are very useful to obtain details before and after adsorption. Aforementioned, physical properties and surface morphology of activated carbons influence adsorption capacity. It is clear from the SEM micrograph in Figure 9 that LAC has a porous surface [See Figure 9(a)]. After adsorption the LAC surface becomes smoother [See Figure 9(b)] implying that components from the red water attach to pores of the LAC.

Adsorption Mechanism

The adsorption performance of LAC is evaluated based on surface groups type, specific surface area, pore size, and so on. There are many oxygen functional groups such as hydroxyl groups, carboxyl groups, phenolic groups, and inner ester on the surface of LAC for efficient adsorption. Most organic components in red water are polar and therefore are believed to adsorb mainly via hydrogen bonds between LAC and organic materials (See Figure 10). According to results, the phenomenon is mainly single molecule layer adsorption.
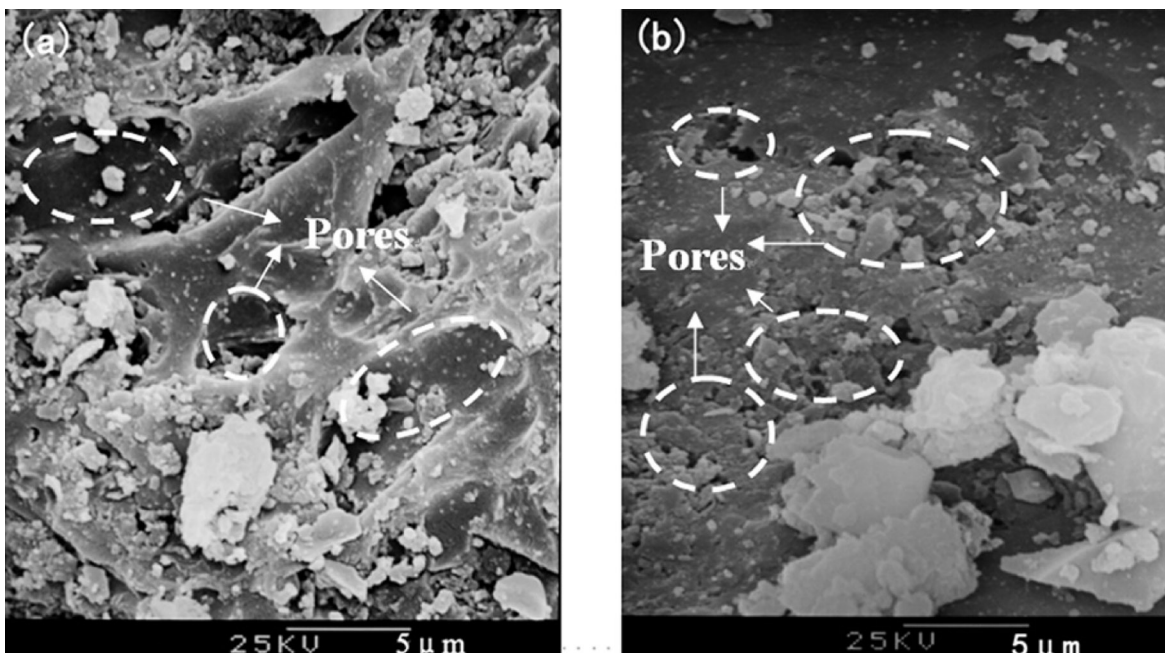

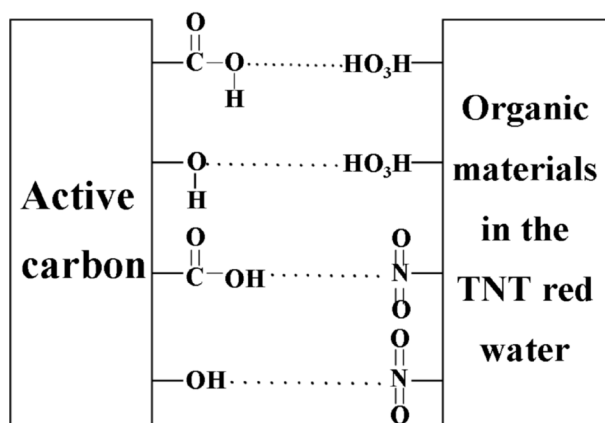***Figure 9.*** *Scanning electron micrographs: (a) LAC (4000×), (b) LAC with adsorbents (1000×).*

Figure 10. *Schematic illustration of hydrogen bonding between active carbon and organic materials in red water.*

Comparison with Other Adsorbents

Several studies have been conducted using various types of adsorbents for TNT adsorption. Table 7 compares adsorption capacities and LAC shows a comparable adsorption capacity with respect to other adsorbents revealing that LAC is suitable for removal of TNT from aqueous solutions since it has a relatively high adsorption capacity.

CONCLUSIONS

Feasibility of using LAC as an adsorbent to remove TNT from red water was investigated. Results demonstrate that pH value, initial concentration, time, and dose of adsorbent all affect adsorption, significantly. The lower the pH the higher the adsorption capacity. Optimal adsorption time is 6 hours and room temperature is adequate. The adsorption mechanism follows a pseudo-second-order kinetics model controlled by pore diffusion and the adsorption isotherm may be fitted well by the Langmuir model. Results suggest organic materials in red water adsorb via hydrogen bonds between activated carbon and organic materials.

ACKNOLEDGEMENTS

Table 7. Adsorption Capacity of TNT by Various Adsorbents.

Adsorbent	Q_e(mg g^{-1})	Reference
LAC	163.79	This study
Aminated lignin	55.7	Zhang *et al*. [30]
polyvinylbenzyl acid/SiO$_2$	26.84	An *et al*. [31]
PEI/SiO$_2$	14.47	An *et al*. [32]
PAM/SiO$_2$	0.873	An *et al*. [33]

REFERENCES

1. Barreto-Rodrigues, M., Silva, F.T., Paiva, T.C.B., Characterization of wastewater from the Brazilian TNT industry, *J. Hazard. Mater.,* 164, 1, 2009, pp. 385–388.
2. Acharya, P., Process Challenges and Evaluation of Bed Agglomeration in a Circulating Bed Combustion System Incinerating Red Water, *Environ. Prog.,* 16 1, 1997, pp. 54–64.
3. Lee, B., Lee, M., Decomposition of 2,4,6-trinitrotoluene (TNT) by gamma irradiation, *Environ. Sci. Technol.,* 39, 23, 2005, pp. 9278–9285.
4. Lee, K.B., Gu, M.B., Moon, S.H., Degradation of 2,4,6-trinitrotoluene by immobilized horseradish peroxidase and electrogenerated peroxide, *Water Res.,* 37, 5, 2003, pp. 983–992.
5. Prak, D.J.L., Solubilization of nitrotoluenes in micellar nonionic surfactant solutions, *Chemosphere,* 68, 10, 2007, pp.1961–1967.
6. Adrian, N.R. and Arnett, C.M., Anaerobic biotransformation of explosives in aquifer slurries amended with ethanol and propylene glycol, *Chemosphere,* 66, 10, 2007, pp. 1849–1856.
7. Rajagopal, C., Kapoor, J.C., Development of adsorptive removal process for treatment of explosives contaminated wastewater using activated carbon, *J. Hazard. Mater.,* 87, 1-3, 2001, pp.73–98.
8. Lee, J.W., Yang, T.H., Shim, W.G., Kwon, T.O., Moon, I.S., Equilibria and dynamics of liquid-phase trinitrotoluene adsorption on granular activated carbon:effect of temperature and pH, *J. Hazard. Mater.,* 141, 1, 2007, pp. 185–192.
9. Tang, W.Y., Zhou, S.F., Wang, L.J., Peng, Q.T., Mechanism study of biodegradation TNT wastewater, *Proceedings of the 3rd International Symposium on Pyrotechnics and Explosives;* Beijing; 1995, pp. 267–270.
10. Wu, Y.G., Jiao, J., Zhao, D.W., Advanced oxidation processes for treatment of wastewater contaminated by explosives, *J. Energetic. Mater.,* 11, 6, 2003, pp.166–169.
11. Chang, S.J., Liu, Y.C., Degradation mechanism of 2,4,6-trinitrotoluene in supercritical water oxidation, *J. Environ. Sci.,* 19, 12, 2007, pp. 1430–1435.
12. Son, H.S., Lee, S.J., Cho, I.H., Zoh, K.D., Kinetics and mechanism of TNT degradation in TiO2 photocatalysis, *Chemosphere,* 57, 4, 2004, pp. 309–317.
13. Schmelling, D.C., Gray, K.A., Photocatalytic transformation and mineralization of 2,4,6-trinitrotoluene(TNT)in TiO$_2$ slurries, *Water Res.,* 29, 12, 1995, pp.2651–2662.
14. Pennington, J.C., Brannon, J.M., Environmental fate of explosives, *Thermochim Acta.,* 384, 1-2, 2002, pp. 163–172.
15. [15] Boopathy, R., Manning, J., Montemagno, C., Kulpa, C., Metabolism of 2,4,6-trinitrotoluene by a Pseudomonas consortium under aerobic conditions, *Curr. Microbiol.,* 28, 3, 1994, pp. 131–137.
16. Lewis, T.A., Newcombe, D.A., Crawford, R.L., Bioremediation of soils contaminated with explosives, *J. Environ. Manage.,* 70, 4, 2004, pp. 291–307.
17. Shen, J.Y., Zhang, J.F., Zuo, Y., Wang, L.J., Sun, X.Y., Li, J.S., Han, W.Q., Biodegradation of 2,4,6-trinitrophenol by Rhodococcus sp isolated from a picric acid contaminated soil, *J. Hazard. Mater.,* 163, 2-3, 2009, pp. 1199–1206.
18. Van Dillewijn, P., Caballero, A., Paz, J.A., Gonzalez-Perez, M.M.,

Oliva, J.M., Ramos, J.L., Bioremediation of 2,4,6-trinitrotoluene under field conditions, *Environ. Sci. Technol.,* 41, 4, 2007, pp. 1378–1383.

19. Bruns-Nagel, D., Drzyzga, O., Steinbach, K., Schmidt, T.C., von Low, E., Gorontzy, T., Blotevogel, K.H., Gemsa, D., Anaerobic/aerobic composting of 2,4,6-trinitrotoluene-contaminated soil in a reactor system, *Environ. Sci. Technol.,* 32, 11, 1998, pp. 1676–1679.

20. Ye, J., Singh, A., Ward, O.P., Biodegradation of nitroaromatics and other nitrogen-containing xenobiotics, *World J. Microbiol. Biotechnol.,* 20, 2, 2004, pp. 117–135.

21. Maloney, S.W., Adrian, N.R., Hickey, R.F., Heine, R.L., Anaerobic treatment of pinkwater in a fluidized bed reactor containing GAC, *J. Hazard. Mater.,* 92, 1, 2002, pp. 77–88.

22. Marinovic, V., Ristic, M., Dostanic, M., Dynamic adsorption of trinitrotoluene on granular activated carbon, *J. Hazard. Mater.,* 117, 2-3, 2005, pp. 121–128.

23. Vasilyeva, G.K., Kreslavski, V.D., Shea, P.J., Catalytic oxidation of TNT by activated carbon, *Chemosphere,* 47, 3, 2002, pp. 311–317.

24. Nefso, E.K., Burns, S.E., McGrath, C.J., Degradation kinetics of TNT in the presence of six mineral surfaces and ferrous iron, *J. Hazard. Mater.,* 123, 1-3, 2005, pp. 79–88.

25. Park. C., Kim, T.H., Kim, S., Kim, S.W., Lee, J., Kim, S.H., Optimization for biodegradation of 2,4,6-trinitrotoluene(TNT), *J. Biosci. Bioeng.,* 95, 6, 2003, pp. 567–571.

26. Weber Jr, W.J., Morris, J.C., Kinetics of adsorption on carbon from solution, *J. Sanit. Eng. Div.,* 89, 2, 1963, pp. 31–59.

27. Ayoub, K., van Hullebusch, E.D., Cassir, M., Bermond, A., Application of advanced oxidation processes for TNT removal: A review, *J. Hazard. Mater.,* 178, 1-3, 2010, pp. 10–28.

28. Namasivayam, C., Yamuna, R.T., Adsorption of chromium (VI) by a low-cost adsorbent: biogas residual slurry, *Chemosphere,* 30, 3, 1995, pp. 561–578.

29. Larous, S., Meniai, A.H., Lehocine, M.B., Experimental study of the removal of copper from aqueous solutions by adsorption using sawdust, *Desalination,* 185, 1-3, 2005, pp. 483–490.

30. Zhang, J.P., Lin, X.Y., Luo, X.G., Zhang, C., Zhu, H., A modified lignin adsorbent for the removal of 2,4,6-trinitrotoluene, *Chem. Eng. J.,* 168, 3, 2011, pp. 1055–1063.

31. An, F.Q., Feng, X.Q., Gao, B.J., Adsorption mechanism and property of a novel adsorption material PAM/SiO(2) towards 2,4,6-trinitrotoluene, *J. Hazard. Mater.,* 168, 1, 2009, pp. 352–357.

32. An, F.Q., Gao, B.J., Feng, X.Q., Adsorption of 2,4,6-trinitrotoluene on a novel adsorption material PEI/SiO(2), *J. Hazard. Mater.,* 166, 2-3, 2009, pp. 757–761.

33. An, F.Q., Gao, B.J., Feng, X.Q., Adsorption performance and mechanism of 2,4,6-trinitrotoluene on a novel adsorption material polyvinylbenzyl acid/SiO(2), *Appl. Surf. Sci.,* 255, 9, 2009, pp. 5031–5035.

GUIDE TO AUTHORS

1. Manuscripts shall be sent electronically to the Editor-in-Chief, Dr. P. Brent Duncan at pduncan@unt.edu using Microsoft Word in an IBM/PC format. If electronic submission is not possible, three paper copies of double-spaced manuscripts may be sent to Dr. P. Brent Duncan, (Editor of the *Journal of Residuals Science & Technology*, University of North Texas, Biology Building, Rm 210, 1510 Chestnut St., Denton, TX 76203-5017) (Tel: 940-565-4350). Manuscripts should normally be limited to the space equivalent of 6,000 words. The editor may waive this requirement in special occasions. As a guideline, each page of a double-spaced manuscript contains about 300 words. Include on the title page the names, affiliations, and addresses of all the authors, and identify one author as the corresponding author. Because communication between the editor and the authors will be electronic, the email address of the corresponding author is required. Papers under review, accepted for publication, or published elsewhere in journals are normally not accepted for publication in the *Journal of Residuals Science & Technology*. Papers published as proceedings of conferences are welcomed.

2. Article titles should be brief, followed by the author's name(s), affiliation, address, country, and postal code (zip) of author(s). Indicate to whom correspondence and proofs should be sent, including telephone and fax numbers and e-mail address.

3. Include a 100-word or less abstract and at least six keywords.

4. If electronic art files are not supplied, submit three copies of camera-ready drawings and glossy photographs. Drawings should be uniformly sized, if possible, planned for 50% reduction. Art that is sent electronically should be saved in either a .tif or .JPEG files for superior reproduction. All illustrations of any kind must be numbered and mentioned in the text. Captions for illustrations should all be typed on a separate sheet(s) and should be understandable without reference to the text.

5. DEStech uses a numbered reference system consisting of two elements: a numbered list of all references and (in the text itself) numbers in brackets that correspond to the list. At the end of your article, please supply a numbered list of all references (books, journals, web sites etc.). References on the list should be in the form given below. In the text write the number in brackets corresponding to the reference on the list. Place the number in brackets inside the final period of the sentence cited by the reference. Here is an example [2].

   Journal: 1. Halpin, J. C., "article title", *J. Cellular Plastics,* Vol. 3, No. 2, 1997, pp. 432–435.

   Book: 2. Kececioglu, D. B. and F.-B. Sun. 2002. *Burn-In Testing: Its Quantification and Optimization,* Lancaster, PA: DEStech Publications, Inc.

6. Tables. Number consecutively and insert closest to where first mentioned in text or type on a numbered, separate page. Please use Arabic numerals and supply a heading. Column headings should be explanatory and carry units. (See example at right.)

Table 5. Comparison of state-of-the-art matrix resins with VPSP/BMI copolymers.

Resin System	Core Temp. (DSC peak)	T_E	Char Yield, %
Epoxy (MY720)	235	250	30
Bismaleimide (H795)	282	>400	48
VPSP/Bismaleimide copolymer			
C379: H795 = 1.9	245	>400	50
C379: H795 = 1.4	285	>400	53

7. Units & Abbreviations. Metric units are preferred. English units or other equivalents should appear in parentheses if necessary.

8. Symbols. A list of symbols used and their meanings should be included.

9. Page proofs. Authors will receive page proofs by E-mail. Proof pages will be in a .PDF file, which can be read by Acrobat Reader. Corrections on proof pages should be limited to the correction of errors. Authors should print out pages that require corrections and mark the corrections on the printed pages. Pages with corrections should be returned by FAX (717-509-6100) or mail to the publisher (DEStech Publications, Inc., 439 North Duke Street, Lancaster, PA 17602, USA). If authors cannot handle proofs in a .PDF file format, please notify the Editor, Dr. P. Brent Duncan at pduncan@unt.edu.

10. Index terms. With proof pages authors will receive a form for listing key words that will appear in the index. Please fill out this form with index terms and return it.

11. Copyright Information. All original journal articles are copyrighted in the name of DEStech Publications, Inc. All original articles accepted for publication must be accompanied by a signed copyright transfer agreement available from the journal editor. Previously copyrighted material used in an article can be published with the *written* permission of the copyright holder (see #14 below).

12. Headings. Your article should be structured with unnumbered headings. Normally two headings are used as follows:

   Main Subhead: DESIGN OF A MICROWAVE INSTALLATION Secondary Subhead: Principle of the Design Method

   If further subordination is required, please limit to no more than one (*Third Subhead*).

13. Equations. Number equations with Arabic numbers enclosed in parentheses at the right-hand margin. Type superscripts and subscripts clearly above or below the baseline, or mark them with a caret. Be sure that all symbols, letters, and numbers are distinguishable (e.g., "oh" or zero, one or lowercase "el," "vee" or Greek nu).

14. Permissions. The author of a paper is responsible for obtaining releases for the use of copyrighted figures, tables, or excerpts longer than 200 words used in his/her paper. Copyright releases are permissions to reprint previously copyrighted material. Releases must be obtained from the copyright holder, which is usually a publisher. Forms for copyright release will be sent by the editor to authors on request.

General: The *Journal of Residuals Science & Technology* and DEStech Publications, Inc. are not responsible for the views expressed by individual contributors in articles published in the journal.